Research Square

Preprints are preliminary reports that have not undergone peer review.
They should not be considered conclusive, used to inform clinical practice,
or referenced by the media as validated information.

Carbon fraction-specific microbial–mineral regulation outweighs direct calcium control in carbonate karst soils

Mubarak Mubarak Ibrahim
Institute of Mountain Hazards and Environment
Chunpei Li
Institute of Mountain Hazards and Environment
Junfang Cui
Institute of Mountain Hazards and Environment
Mei Lu
Institute of Mountain Hazards and Environment
Jigao Wang
Guizhou Academy of Agricultural Sciences
Jie Zhang
Institute of Mountain Hazards and Environment
Wei Tian
Yangtze University
Jialiang Tang
jtang@imde.ac.cn

Institute of Mountain Hazards and Environment

Research Article

Keywords: Karst soils, soil organic carbon fractions, mineral-associated organic carbon, particulate organic carbon, calcium geochemistry, microbial–mineral interactions

Posted Date: September 13th, 2026

DOI: https://doi.org/10.21203/rs.3.rs-10891998/v1

License: This work is licensed under a Creative Commons Attribution 4.0 International License.
Read Full License

Additional Declarations: No competing interests reported.

Abstract

Purpose

Carbon accumulation and persistence in karst soils is governed by interacting biological and mineral processes, yet the relative roles of microbial regulation, mineral protection, and calcium-mediated stabilization remain poorly constrained. Here, we investigated SOC pools and their fraction-specific controls across contrasting limestone and dolomite soils in southwest China.

Methods

We combined SOC fractionation with measurements of microbial biomass and community characteristics, calcium geochemistry, and mineral-associated properties. Boosted regression trees (BRT) and partial least squares structural equation modeling (PLS-SEM) were used to assess the relative importance and interconnected associations of these properties with SOC, mineral-associated organic carbon (MAOC), and particulate organic carbon (POC).

Results

SOC pools differed among carbonate lithologies and sites, with Puding dolomite soils exhibiting the highest SOC, MAOC, and POC concentrations alongside enhanced microbial biomass and mineral surface capacity. Microbial properties were the dominant predictors of carbon fractions, accounting for 79.1%, 62.1%, and 92.5% of BRT importance for SOC, MAOC, and POC respectively, strongest for POC. MAOC was jointly regulated by microbial and mineral properties, particularly cation exchange capacity and reactive Fe–Al phases. In contrast, calcium fractions showed no significant direct effects on carbon pools and contributed 3% or less BRT importance across all fractions.

Conclusion

SOC storage in carbonate karst soils is more strongly associated with fraction-specific microbial and mineral-associated pathways than with direct calcium effects. These findings highlight the value of representing POC and MAOC separately and distinguishing microbial, mineral-associated, and calcium-related pathways when conceptualizing soil C cycling in karst soils.

1. Introduction

Soil organic carbon (SOC) persistence is increasingly understood to depend not simply on the chemical recalcitrance of organic inputs, but on the pathways through which carbon is processed and protected within the soil matrix (Schmidt et al. 2011; Barré et al. 2018; Sokol et al. 2019, 2022). A useful process-based distinction separates SOC into particulate organic carbon (POC) and mineral-associated organic

carbon (MAOC), which differ in formation, turnover, and sensitivity to environmental change (Cotrufo et al. 2019; Lavallee et al. 2020). POC is composed largely of relatively coarse plant-derived residues and microbial products whose persistence depends strongly on input rates, decomposition, and physical protection, whereas MAOC consists of smaller organic compounds associated with mineral surfaces and generally exhibits longer turnover (Sokol and Bradford 2019; Haddix et al. 2020; Witzgall et al. 2021). Consequently, similar total SOC stocks can arise from fundamentally different stabilization mechanisms (Zhou et al. 2024). Therefore, disentangling the controls on MAOC and POC is essential for predicting both the magnitude and the long-term persistence of soil carbon storage (Cotrufo et al. 2019; Lavallee et al. 2020).

Microbial transformation of organic inputs and physicochemical protection by minerals are two processes increasingly recognized as central to SOC partitioning and persistence (Six et al. 2002). Microbial-explicit frameworks emphasize that microorganisms convert plant-derived substrates into biomass, metabolites, extracellular products, and necromass that subsequently contribute to SOC formation (Cotrufo et al. 2013; Kallenbach et al. 2016; Liang et al. 2017). Global analyses further demonstrate strong links among microbial biomass, carbon-use efficiency, necromass production, and SOC accumulation (Wang et al. 2021a; Tao et al. 2023). However, microbial products are more likely to persist when their accessibility to decomposers is reduced or when they become associated with reactive mineral surfaces (Kleber et al. 2015). Mineralogical properties, including exchange capacity, poorly crystalline Fe and Al phases, surface area, and mineral saturation, can therefore regulate the retention of microbially processed carbon, particularly within MAOC (Rasmussen et al. 2018; Georgiou et al. 2022). This coupled perspective has shifted SOC research away from treating biological inputs and mineral protection as competing explanations toward viewing them as sequential and interacting controls on carbon formation and persistence.

Karst soils of southwest China develop predominantly from limestone and dolomite and are characterized by heterogeneous soil depth, high carbonate-derived base-cation availability, discontinuous soil–rock interfaces, and strong spatial variability in water and nutrient availability (Wang et al. 2019). Calcium has therefore received particular attention as a potential SOC-stabilizing factor (Rowley et al. 2018; Shabtai et al. 2023). Ca^{2+} can promote aggregation, reduce organic-matter solubility, and bridge negatively charged organic functional groups with mineral surfaces, providing plausible direct mechanisms of SOC protection (Rowley et al. 2018; Dou et al. 2024). More recent experimental studies indicate that calcium can also modify microbial colonization and transformation of plant litter, suggesting that its influence may extend beyond direct organo-mineral bonding to biological pathways (Shabtai et al. 2023; Xiao et al. 2026). At the same time, reactive Fe–Al phases and soil aggregates can exert strong control over microbial-derived carbon in karst soils, and lithology can alter microbial carbon-use efficiency, necromass production, and subsequent mineral protection (Hu et al. 2022b, 2024; Xie et al. 2024). Thus, high calcium availability does not necessarily imply that calcium is the dominant proximate control of SOC accumulation.

Research in southwest Chinese karst ecosystems has established that SOC varies substantially with vegetation development, land use, topography, nutrient availability, microbial activity, and bedrock lithology (Liu et al. 2015; Chen et al. 2018, 2019a; Wang et al. 2018). Importantly, limestone and dolomite cannot be assumed to generate equivalent carbon-cycling environments. Density-fraction studies have reported lithological differences in bulk SOC and heavy-fraction carbon between limestone- and dolomite-derived soils (Wen et al. 2017), while microbial C limitation also differs between the two carbonate substrates (Chen et al. 2019a). More recent studies have shown that carbonate lithology can alter aggregate protection, mineral interactions, microbial C processing, and necromass stabilization (Xie et al. 2024; Hu et al. 2024; Lin et al. 2025). However, these research streams remain only partly integrated. Much of the karst literature has focused on bulk SOC, vegetation or land-use gradients, microbial necromass, or comparisons between carbonate and non-carbonate soils. Comparatively less is known about the relative and interconnected roles of living microbial biomass and community attributes, reactive mineral properties, and distinct calcium pools in regulating POC and MAOC within contrasting carbonate lithologies. In particular, it remains unclear whether the Ca-rich geochemical environment characteristic of karst soils exerts dominant direct control when microbial and mineral pathways are considered simultaneously.

To address this gap, we investigated soils developed from limestone and dolomite at Puding and Zunyi in southwest China and quantified SOC, MAOC, and POC together with microbial biomass and PLFA community attributes, CEC, operationally defined Fe–Al mineral phases, and multiple calcium fractions. We aimed to evaluate the relative and interconnected associations of microbial properties, mineral-associated properties, and calcium geochemistry with SOC, MAOC, and POC across contrasting carbonate lithologies. We hypothesized, first, that microbial and mineral-associated properties would jointly explain variation in SOC pools, with their relative influence differing between MAOC and POC. Second, we hypothesized that calcium geochemistry would exert a dominant direct influence on SOC, MAOC, and POC in carbonate karst soils. This framework allows direct Ca–carbon associations to be evaluated alongside microbial and mineral-associated pathways and provides a fraction-specific assessment of the processes associated with SOC storage across contrasting carbonate lithologies.

2 Methodology

2.1 Study area and soil sampling

The study was conducted in the karst region of Guizhou Province, southwest China (26°22'–27°34' N, 105°46'–106°59' E). The region has a subtropical monsoon climate, with mean annual precipitation of 1089.87–1161.24 mm, mean annual temperature of 15.74–16.35°C, and elevations ranging from 836 to 1245 m a.s.l. (Table S1). Site-specific climatic data were obtained from the National Earth System Science Data Center, National Science & Technology Infrastructure of China, using a 1-km gridded climate dataset for 1901–2023.

Two sites, Puding (P) and Zunyi (Z), were selected, each containing soils developed from dolomite (D) and limestone (L), giving four site–lithology settings: Puding–Dolomite (PD), Puding–Limestone (PL), Zunyi–Dolomite (ZD), and Zunyi–Limestone (ZL). Within each setting, three slope positions (upper, middle, and lower) were selected. At each slope position, three independent composite soil samples were collected, resulting in nine samples per setting and 36 samples in total. At each sampling location, a 5 × 5 m plot was established while avoiding field margins, streams, and drainage channels. Surface litter was removed, and five soil cores were randomly collected from the 0–30 cm mineral layer and homogenized into one composite sample. Each sample was divided into two portions. Fresh soil was transported to the laboratory in insulated containers with ice packs for microbial biomass and PLFA analyses, whereas the remaining soil was air-dried at approximately 25°C and sieved to < 2 mm for physicochemical, carbon-fraction, and mineral analyses. Vegetation type, slope aspect, and bedrock exposure were recorded in the field (Table S1). Soil sampling was conducted in July 2024.

2.2 Soil physicochemical properties and organic carbon fractions

Soil physicochemical properties were determined following standard methods (Lu 2000). Soil pH was measured in a 1:2.5 soil:water suspension using a calibrated pH meter. Soil moisture was determined gravimetrically by oven drying at 105°C, and bulk density was measured using a 100-cm³ core. Particle-size distribution was determined by the pipette–gravimetric method. Total nitrogen (TN) was measured by the micro-Kjeldahl method. Total phosphorus (TP) was determined colorimetrically using the molybdenum-blue method following H_2SO_4–$HClO_4$ digestion. KCl-extractable available nitrogen (AN) was determined from fresh soil within 48 h of sampling using 2 M KCl at a soil:solution ratio of 1:5 (w/v), followed by quantification using an AA3 continuous-flow analyzer (SEAL Analytical, Germany). Cation exchange capacity (CEC) was determined using the ammonium chloride–ammonium acetate method appropriate for calcareous soils (Lu 2000).

SOC was determined after removal of inorganic carbon with HCl using potassium dichromate oxidation (Lu 2000). POC and MAOC were separated by physical size fractionation following established SOC-fractionation procedures (Poeplau et al. 2018). Briefly, 10 g of air-dried soil was dispersed in 30 mL of 5 g L^{-1} sodium hexametaphosphate and shaken for 18 h before wet sieving at 53 μm. The > 53 μm fraction was collected as particulate organic matter, whereas the < 53 μm fraction was collected as mineral-associated organic matter. Both fractions were dried and weighed, treated with 1 M HCl to remove inorganic carbon, and analyzed for organic C by potassium dichromate oxidation. POC and MAOC concentrations on a bulk-soil basis were calculated from the C concentration and dry-mass proportion of the corresponding fraction and expressed as g C kg^{-1} dry soil.

2.3 Calcium fractions and Fe–Al mineral phases

Soil $CaCO_3$ was determined by calcimetry. Exchangeable Ca^{2+} (E-Ca^{2+}) was extracted using the ammonium chloride–ammonium acetate method, whereas sulfate-extractable Ca (Ca□) was extracted

using 0.5 M Na_2SO_4 (Wang et al. 2021b). Calcium concentrations in the extracts were quantified by inductively coupled plasma atomic emission spectrometry (ICP-AES).

Free pedogenic Fe and Al (Fed and Ald) were extracted using citrate–bicarbonate–dithionite solution, poorly crystalline Fe and Al (Feo and Alo) were extracted using acid ammonium oxalate, and organically complexed Fe and Al (Fep and Alp) were extracted using sodium pyrophosphate (Lu 2000; Chen et al. 2019b). Fe and Al concentrations in all extracts were determined by ICP-AES. The operational mineral indices (0.5Fed + Ald), (0.5Feo + Alo), and (0.5Fep + Alp) were used in subsequent analyses.

2.4 Microbial biomass and phospholipid fatty acids

Microbial biomass carbon (MBC) was determined in fresh soil by chloroform fumigation followed by K_2SO_4 extraction according to Lu (2000) and expressed as g C kg^{-1} dry soil.

Microbial community biomass and composition were characterized using phospholipid fatty acid (PLFA) analysis. PLFAs were extracted from 5.00 g of freeze-dried soil using a chloroform-methanol-citric acid buffer solution. The extracted phospholipids were converted to fatty acid methyl esters (FAMEs) and analyzed by gas chromatography (Agilent 7890, Santa Clara, USA) equipped with a flame ionization detector (Fierer et al. 2003; Zhu et al. 2024). PLFA peaks were identified using bacterial fatty acid standards and MIDI peak identification software (MIDI, Inc., Newark, DE) and named following the nomenclature of Frostegård et al. (1993). PLFAs were classified into Gram-positive bacterial biomass (G+ PLFAs), Gram-negative bacterial biomass (G– PLFAs), Actinomycetes biomass, total bacterial PLFAs, fungal PLFAs, and total microbial PLFAs (Frostegård et al. 1993; Zhu et al. 2024).

2.5 Statistical analyses

Variables that did not meet assumptions of normality and homogeneity of variance were natural-log-transformed prior to analysis. A full factorial three-way ANOVA with Site, Rock type, and Slope position was performed to assess main effects and interactions; results are provided in Supplementary Table S2. Differences among PD, PL, ZD, ZL were evaluated using one-way ANOVA followed by Fisher's LSD post-hoc test at $p < 0.05$. Within-site lithological contrasts (PD vs. PL; ZD vs. ZL) and site contrasts within each lithology (PD vs. ZD; PL vs. ZL) were tested using independent-samples t-tests. Lithology-stratified linear regressions were performed separately for dolomite- and limestone-derived soils to quantify predictor–carbon relationships. Differences in regression slopes between lithologies were tested using ANCOVA models including Site as a fixed factor to control for site-level effects, with the predictor × lithology interaction used to test slope differences. Boosted regression tree (BRT) analysis was performed following Elith et al. (2008) using the gbm package in R to quantify the relative importance of individual predictors and predictor groups (Calcium, Mineral, Microbial) for SOC, MAOC, and POC, using 5-fold cross-validation, 5000 trees, a learning rate of 0.01, and tree complexity of 3. Partial least squares structural equation modeling (PLS-SEM) was conducted using the plspm package to evaluate direct and indirect pathways among rock type, calcium properties, mineral properties, microbial properties, and carbon fractions, with 500 bootstrap resamples used for significance testing of path coefficients. The

variance inflation factor (VIF) was calculated for all predictors prior to model construction; variables with VIF > 10 were excluded (Table S3). All analyses were performed in R 4.4.3.

3 Results

3.1 Carbon pools and soil physicochemical characteristics

Three-way ANOVA showed no significant interactive effects of slope position with site or lithology on any measured variable; detailed slope-position effects are therefore reported in Table S2 but are not discussed further. SOC, MAOC, and POC differed significantly among treatments (all $p < 0.001$; Fig. 1). PD had the highest carbon concentrations (SOC: 42.84 ± 3.29; MAOC: 30.73 ± 2.03; POC: 12.31 ± 1.63 g kg^{-1}), significantly exceeding PL, ZD, and ZL ($p < 0.05$), which did not differ significantly from one another. Within-site t-tests showed significant lithological differences only at Puding (PD > PL for all fractions; all $p < 0.001$), while ZD and ZL did not differ significantly for any carbon fraction.

Soil pH was stable across treatments (7.64–7.92; Table 1). Moisture was higher in Puding than Zunyi soils, and BD was lowest in PD. TN and AN were significantly higher in PD than in the other settings, whereas TP was highest in PD but did not differ significantly from ZD (Table 1). Clay content was highest in ZD (18.32 ± 0.74%) and lowest in PL (7.60 ± 0.46%), while silt did not differ significantly among treatments.

Table 1
Soil physicochemical properties across treatments

Variable	PD	PL	ZD	ZL
pH	7.88 ± 0.05 a	7.92 ± 0.05 a	7.64 ± 0.13 a	7.66 ± 0.10 a
Moisture (%)	24 ± 1.00 a	25 ± 1.00 a	17 ± 1.00 b	13 ± 1.00 c
BD (g cm^{-3})	0.98 ± 0.03 b	1.12 ± 0.03 a	1.17 ± 0.03 a	1.13 ± 0.03 a
TN (g kg^{-1})	4.18 ± 0.39 a	2.36 ± 0.24 b	2.07 ± 0.10 b	1.71 ± 0.15 b
TP (g kg^{-1})	0.68 ± 0.06 a	0.52 ± 0.03 b	0.61 ± 0.04 ab	0.30 ± 0.02 c
AN (g kg^{-1})	0.41 ± 0.04 a	0.26 ± 0.02 b	0.21 ± 0.01 b	0.19 ± 0.01 b
Sand (%)	19.40 ± 1.49 b	23.74 ± 0.70 a	13.82 ± 1.13 c	23.40 ± 1.20 a
Silt (%)	69.52 ± 1.06 a	68.66 ± 0.61 a	67.86 ± 0.68 a	68.20 ± 0.75 a
Clay (%)	11.08 ± 1.60 b	7.60 ± 0.46 c	18.32 ± 0.74 a	8.40 ± 0.83 bc

Note: (PD = Puding Dolomite, PL = Puding Limestone, ZD = Zunyi Dolomite, ZL = Zunyi Limestone). Values are means ± standard error (n = 9). Different lowercase letters within a row indicate significant differences among treatments (one-way ANOVA with LSD post-hoc test, $p < 0.05$). BD = bulk density; TN = total nitrogen; TP = total phosphorus; AN = available nitrogen.

3.2 Microbial community characteristics

Microbial biomass and community composition differed significantly among treatments (Table 2; Fig. 2). PD had the highest MBC and most PLFA group abundances. MBC in PD (0.77 ± 0.10 g kg^{-1}) significantly exceeded PL, ZD, and ZL ($p < 0.001$). Total PLFA (206.81 ± 25.21 nmol g^{-1}) and bacterial PLFA (179.39 ± 21.27 nmol g^{-1}) were both significantly higher in PD than in all other treatments ($p < 0.05$), while ZD, ZL, and PL did not differ significantly. Fungal PLFA was highest in PD (27.42 ± 4.66 nmol g^{-1}) and lowest in PL (10.87 ± 2.50 nmol g^{-1}; $p = 0.027$). GP, GN, and Actinomycetes all followed the same pattern, with PD significantly exceeding the remaining treatments. The F:B ratio was highest in ZL (0.20 ± 0.02) and lowest in PL (0.11 ± 0.02), while the GP:GN ratio did not differ significantly among treatments (range: 1.15–1.27; Table 2).

Lithological effects on microbial properties were significant only at Puding: PD showed significantly higher MBC, bacterial PLFA, total PLFA, GP, GN, and Actinomycetes than PL (all $p < 0.05$), while no significant microbial differences were detected between ZD and ZL.

Table 2
Microbial community properties

Variable	PD	PL	ZD	ZL
Actinomycetes (nmol g^{-1})	46.49 ± 5.93 a	22.97 ± 2.72 b	25.23 ± 2.08 b	22.91 ± 3.81 b
GP (nmol g^{-1})	74.91 ± 9.81 a	38.30 ± 4.64 b	48.50 ± 3.76 b	41.03 ± 6.37 b
GN (nmol g^{-1})	57.99 ± 5.95 a	33.68 ± 4.68 b	39.47 ± 4.05 b	33.11 ± 5.64 b
F:B ratio	0.15 ± 0.01 ab	0.11 ± 0.02 b	0.15 ± 0.02 ab	0.20 ± 0.02 a
GP:GN ratio	1.27 ± 0.09 a	1.15 ± 0.03 a	1.26 ± 0.05 a	1.26 ± 0.06 a

Note: Microbial community properties across treatments (PD = Puding Dolomite, PL = Puding Limestone, ZD = Zunyi Dolomite, ZL = Zunyi Limestone). Values are means ± standard error (n = 9). Different lowercase letters within a row indicate significant differences among treatments (one-way ANOVA with LSD post-hoc test, $p < 0.05$). GP = Gram-positive bacteria; GN = Gram-negative bacteria; F:B = fungal:bacterial ratio; GP:GN = Gram-positive:Gram-negative ratio.

3.3 Mineral and calcium properties

Mineral properties showed stronger treatment differentiation than calcium fractions (Fig. 3; Fig. 4). CEC differed significantly among all treatments ($p < 0.001$), following the hierarchy PD > PL > ZD > ZL. Both 0.5Feo + Alo and 0.5Fed + Ald were significantly higher in Puding than Zunyi soils regardless of lithology (both $p < 0.001$), while 0.5Fep + Alp showed no significant treatment differences ($p = 0.634$). Lithological effects on CEC were significant within both sites (PD > PL; ZD > ZL; $p < 0.05$), whereas Fe–Al oxide fractions did not differ significantly between lithologies at either site.

Among calcium fractions (Fig. 4), only E-Ca^{2+} differed significantly among treatments ($p = 0.027$), with ZD showing the highest value (1.44 ± 0.15 g kg^{-1}) and PL the lowest (0.96 ± 0.03 g kg^{-1}). $CaCO_3$ values ranged widely (2.76–33.49 g kg^{-1}) but the overall treatment effect was not significant ($p = 0.062$), with a within-site difference detected only at Zunyi (ZD > ZL; $p < 0.05$). Ca□ showed no significant variation among treatments.

3.4 Relationships between environmental variables and carbon fractions

Microbial variables showed the strongest and most consistent relationships with carbon fractions across both lithologies (Fig. 5). MBC explained 59.5–83.3% of SOC variance and approximately 57% of MAOC variance in both lithologies (all $p < 0.001$), and was also significantly associated with POC (Dolomite: $R^2 = 0.782$; Limestone: $R^2 = 0.453$). ANCOVA confirmed significant MBC effects on all carbon fractions ($p < 0.001$), with no significant rock type × MBC interactions. Bacterial and total PLFA showed similarly consistent relationships across lithologies for all three fractions, with a significant rock type × bacterial PLFA interaction only for POC ($p = 0.044$). Fungal PLFA explained 40.2% and 85.0% of POC variance in Dolomite and Limestone soils respectively, with no significant rock type interaction.

For mineral properties (Fig. 6), CEC was significantly associated with SOC and MAOC in both lithologies (SOC: $R^2 = 0.574–0.695$; MAOC: $R^2 = 0.742–0.844$; all $p < 0.001$) and with POC only in Dolomite soils ($R^2 = 0.534$, $p < 0.001$), with significant rock type × CEC interactions for all three fractions ($p \leq 0.007$). 0.5Feo + Alo was significantly associated with SOC, MAOC, and POC in Dolomite soils ($R^2 = 0.498–0.582$; all $p < 0.005$) but only with MAOC in Limestone soils ($R^2 = 0.253$, $p = 0.033$), with significant rock type interactions for all three fractions (all $p < 0.001$). 0.5Fed + Ald showed significant relationships only with MAOC in both lithologies, and 0.5Fep + Alp showed no significant relationships with any carbon fraction.

Calcium fractions showed consistently weak associations with carbon fractions (Fig. 7). $CaCO_3$ and Ca□ showed no significant relationships with SOC, MAOC, or POC in either lithology. E-Ca^{2+} was significantly related to POC only in Limestone soils ($R^2 = 0.387$, $p = 0.006$), with no significant rock type interaction terms.

3.5 Relative importance and pathway analysis

BRT models explained 81.4%, 87.4%, and 81.5% of cross-validated variance for SOC, MAOC, and POC respectively (Fig. 8). The Microbial group dominated relative importance for all three fractions (SOC: 79.1%; MAOC: 62.1%; POC: 92.5%). MBC was the single most important predictor for SOC (36.9%) and POC (44.7%), while CEC ranked first for MAOC (30.4%), followed by MBC (20.5%) and bacterial PLFA (11.4%). The Mineral group contributed 34.9% for MAOC but only 5.3% for POC. Calcium variables contributed 3.0% or less across all three fractions.

The PLS-SEM model explained 79%, 83%, and 80% of the variance in SOC, MAOC, and POC, respectively (GoF = 0.663; Fig. 9). Parent rock type showed strong positive paths to calcium properties (β = 0.91) and mineral properties (β = 0.65), whereas its path to microbial properties was nonsignificant. Mineral properties showed a significant positive path to microbial properties (β = 0.48) and significant direct paths to SOC (β = 0.40) and MAOC (β = 0.58), resulting in the largest modeled total effect on MAOC. Calcium properties showed no significant direct paths to SOC, MAOC, or POC but exhibited smaller indirect associations, primarily through microbial properties (total indirect effects = 0.143–0.275). Microbial properties showed significant positive paths to all three carbon fractions, with the strongest path to POC (β = 0.90; total effect = 0.904). VIF values for all retained indicators were below 10 (Table S3).

4. Discussion

Our study indicates that SOC storage in carbonate karst soils is more strongly associated with microbial carbon processing and mineral-associated properties than with direct calcium-mediated effects. Although carbonate lithology was strongly associated with calcium and mineral properties, the measured calcium fractions showed limited direct relationships with SOC pools. Microbial properties emerged as the strongest predictors across carbon fractions, particularly POC, whereas mineral-associated properties contributed substantially to MAOC. Together, these results indicate that microbial and mineral-associated pathways better explained variation in SOC fractions than the measured calcium properties under the carbonate karst conditions examined here.

4.1 Microbial properties as the dominant biological predictors of SOC pools.

Microbial regulation was evident across all carbon fractions but was strongest for POC. Microbial properties accounted for 79.1%, 62.1%, and 92.5% of grouped BRT relative influence for SOC, MAOC, and POC, respectively (Fig. 8). PLS-SEM likewise showed strong direct microbial effects on SOC (β = 0.63) and especially POC (β = 0.90), whereas the microbial effect on MAOC (β = 0.47) was accompanied by a stronger mineral pathway (β = 0.58; Fig. 9). These patterns are consistent with microbial-explicit SOC frameworks in which microorganisms transform plant inputs into biomass, metabolites, and residues that can subsequently enter persistent soil pools (Cotrufo et al. 2013; Kallenbach et al. 2016; Liang et al. 2017). Global syntheses further show that microbial necromass can constitute a substantial fraction of SOC and generally increases with living microbial biomass (Liang et al. 2019; Wang et al. 2021a). Karst studies provide direct support for this biological pathway. At the Puding Karst Critical Zone Observatory, microbial residue C accounted for 17–28% of SOC and increased with vegetation recovery together with microbial biomass and soil nutrient status (Guo et al. 2021). Across broader southwest China karst gradients, SOC accrual has also been associated with increasing microbial network complexity and shifts in bacterial ecological strategies rather than microbial diversity alone (Hu et al. 2022a, 2023). Our results complement these restoration-based studies by demonstrating that microbial controls remain

important across naturally contrasting carbonate lithologies. MBC was positively related to SOC, MAOC, and POC in both Dolomite and Limestone soils (Fig. 5), while the absence of significant lithology × MBC interactions (Fig. 5) indicates that the microbial–C association was broadly conserved across the two parent rocks. The particularly strong microbial signal for POC does not demonstrate that POC is solely microbial in origin. Rather, it indicates that particulate C accumulation was closely coupled to the biological processes controlling organic-input transformation and turnover, without establishing the ultimate biological origin of the retained C itself. Recent evidence shows that this coupling is context dependent. Yang et al. (2025) found microbial necromass more strongly associated with POC than MAOC across a regional soil transect, whereas a global biomarker synthesis reported preferential microbial-necromass retention in MAOM, particularly in forests (Xuan et al. 2024). Importantly for karst systems, Zhu et al. (2026) found substantial microbial-necromass accumulation in both POC and MAOC following afforestation of calcareous soils. Thus, our high microbial relative influence for POC is best interpreted as strong biological regulation of the particulate pool, while entry of microbial-derived C into MAOC additionally depends on mineral retention. The PD–ZD contrast further shows that this microbial pathway cannot be attributed to lithology alone. Both soils developed from Dolomite, yet PD combined higher moisture and TN (Table 1) with greater MBC, bacterial PLFA, GP bacteria, and Actinomycetes (Fig. 2; Table 2) and the largest SOC fractions (Fig. 1). Similar covariation among nutrient availability, microbial biomass, and SOC has been reported during karst recovery (Guo et al. 2021; Hu et al. 2023). Community composition also contributed information beyond total biomass: GP bacteria and Actinomycetes were enriched in PD and ranked among the microbial predictors of SOC in BRT (Fig. 8). However, PLFA biomarkers indicate broad living-community structure rather than taxon-specific C stabilization functions. Accordingly, these community shifts should be interpreted as accompanying greater microbial processing capacity, not as direct evidence that particular groups produced the accumulated persistent C. This distinction may also explain why the higher F:B ratio in ZL (Table 2) did not correspond to greater carbon storage. Overall, microbial biomass and community structure emerged as the dominant biological correlates of SOC pools, while their relative influence differed between POC and MAOC.

4.2 Mineral-associated properties contribute to MAOC through microbial–mineral coupling

Mineral regulation was concentrated mainly in MAOC rather than POC. Mineral properties accounted for 34.9% of grouped BRT relative influence for MAOC but only 5.3% for POC (Fig. 8). Likewise, the Mineral construct had a strong direct effect on MAOC ($\beta = 0.58$, $p < 0.001$) but not on POC ($\beta = 0.04$; Fig. 9). This fraction-specific response indicates that mineral properties were particularly important for retaining C in mineral-associated forms rather than increasing all SOC fractions uniformly. This agrees with the POM–MAOM framework, which identifies mineral association and restricted microbial accessibility as major mechanisms of MAOM persistence, whereas POM remains comparatively less associated with reactive mineral surfaces (Lavallee et al. 2020). Among the measured mineral-related properties, CEC showed the most consistent association with MAOC. It explained 74.2% and 84.4% of MAOC variation in Dolomite and Limestone soils, respectively (Fig. 6), and had the highest individual relative influence in the MAOC

BRT model (30.4%; Fig. 8). This agreement across analyses identifies the exchange-active soil environment as an important control of MAOC concentrations. CEC should not, however, be interpreted as a direct measure of mineral surface area because both mineral and organic charge sites contribute to exchange capacity in surface soils (Solly et al. 2020). Reactive Fe–Al phases provided more specific evidence of mineral involvement. The 0.5Feo + Alo index was positively associated with all carbon fractions in Dolomite soils but only with MAOC in Limestone soils, with significant lithology interactions (all $p < 0.001$; Fig. 6). Short-range-order Fe and Al phases can protect organic matter through sorption, ligand exchange, co-precipitation, and formation of heterogeneous organo-mineral assemblages (Mikutta et al. 2006; Kögel-Knabner et al. 2008). The lack of relationships involving 0.5Fep + Alp therefore suggests that the oxalate-extractable reactive pool tracked MAOC differentiation more closely than the pyrophosphate-extractable pool, without implying a single stabilization mechanism (Wagai and Mayer 2007). The lithology dependence of these relationships is particularly relevant in karst soils. Lin et al. (2025), working in central Guizhou, found greater SOC storage in dolomite than limestone forest soils and linked this difference to aggregation and clay mineralogy. Their results confirm that dolomite and limestone can generate contrasting physicochemical environments for C retention, although their study emphasized aggregate-associated C whereas our strongest direct mineral signal occurred in MAOC. Recent karst studies further show that the relative roles of aggregates and minerals in microbial necromass retention depend on parent material (Xie et al. 2024), while Hu et al. (2024) demonstrated lithological regulation of microbial C-use efficiency and necromass stabilization through aggregate–mineral interactions. Our PLS-SEM supports this coupled interpretation. Mineral properties positively influenced microbial properties ($\beta = 0.48$, $p < 0.001$), while both Mineral ($\beta = 0.58$) and Microbial ($\beta = 0.47$) properties directly affected MAOC (Fig. 9). Li et al. (2026) similarly reported strong microbial–mineral co-regulation of MAOC in limestone- and dolomite-derived karst soils. Thus, the high MAOC in PD is best interpreted as the concurrence of strong microbial C processing and favourable mineral-associated retention. In contrast, the weak direct mineral effect on POC suggests that this mineral pathway was principally important for MAOC stabilization, while particulate C remained more closely coupled to biological processing.

4.3 Re-evaluating calcium-mediated carbon stabilization in carbonate karst ecosystems

Contrary to our second hypothesis, calcium was not a dominant direct predictor of SOC pools. Calcium variables contributed only 2.6%, 3.0%, and 2.2% of BRT relative influence for SOC, MAOC, and POC, respectively (Fig. 8), and showed no significant direct PLS-SEM effects on any carbon fraction (Fig. 9). Similarly, $CaCO_3$ and Ca□ were unrelated to SOC fractions across both lithologies, while exchangeable Ca^{2+} was associated only with POC in Limestone soils ($R^2 = 0.387$, $p = 0.006$; Fig. 7). The weak overall signal indicates that variation in Ca properties was not a first-order direct predictor of SOC, MAOC, or POC under the carbonate karst conditions examined here. This result does not question the capacity of Ca to stabilize organic matter. Ca^{2+} can enhance aggregation, cation bridging, and organo-mineral association (Rowley et al. 2018), and Ca-rich soils can contain substantially more mineral-associated SOC than comparable Ca-poor soils (Rowley et al. 2021). Recent nanoscale imaging further

demonstrates extensive Ca–organic associations around calcite and other mineral interfaces in alkaline soils (Varga et al. 2025). However, field evidence shows that the strength of this mechanism is context dependent. In southwest China karst forests, Ca-rich bedrock and soil Ca were positively associated with SOM stability (Tang et al. 2023), while exchangeable Ca contributed directly and indirectly to SOC accumulation during karst vegetation restoration (Lan et al. 2025). Conversely, experiments in calcareous soils showed that increasing $CaCO_3$ could enhance SOC mineralization rather than storage (Dou et al. 2024), and that elevated $CaCO_3$ altered SOC fractions together with bacterial community composition (Dou et al. 2023). Thus, the established capacity of Ca to stabilize organic matter does not imply that Ca-mediated processes will dominate SOC accumulation in all carbonate soils. Our PLS-SEM suggests that Ca remained relevant through a biological pathway. Calcium positively influenced microbial properties ($\beta = 0.31$, $p < 0.05$; Fig. 9), whereas its direct carbon pathways were non-significant. Experimental isotope tracing provides mechanistic support: Ca addition altered microbial community composition and increased litter-C incorporation into microbial biomass and microbial C-use efficiency (Shabtai et al. 2023). Karst restoration studies likewise link exchangeable Ca^{2+} to microbial community reassembly, necromass accumulation, and aggregate-associated C formation (Lan et al. 2025; Xiao et al. 2026). Together, these findings support a more conditional interpretation of Ca in our system: Ca may facilitate carbon accumulation partly by modifying the microbial and physicochemical environment, but it was not the dominant direct stabilizing pathway. Under the carbonate karst conditions examined here, microbial and mineral properties discriminated SOC fractions more strongly than Ca abundance, while Ca showed a smaller, predominantly indirect modeled contribution (Fig. 8; Fig. 9). These interpretations should nevertheless be viewed within the constraints of the observational design and modelling approaches. Differences in land use among some site–parent rock settings preclude attribution of all observed contrasts solely to lithology. In addition, BRT relative influence and PLS-SEM pathways should not be interpreted as causal effects because both depend on the predictor set and model specification (Elith et al. 2008; Danks et al. 2020). Nevertheless, the consistency of the fraction-specific patterns across lithology-stratified regressions, BRT, and PLS-SEM provides convergent evidence for the relative importance of microbial and mineral controls. Future work combining microbial necromass biomarkers, isotope tracing, and direct characterization of organo-mineral and Ca–organic associations would provide the mechanistic tests required to resolve these pathways.

5 Conclusion

This study shows that SOC storage in carbonate karst soils is more strongly associated with coordinated microbial and mineral pathways than with direct calcium-mediated effects. Across contrasting limestone- and dolomite-derived soils, microbial properties were the strongest predictors of SOC fractions, particularly POC, whereas mineral-associated properties contributed substantially to MAOC. Calcium properties showed no significant direct effects on SOC, MAOC, or POC and instead exhibited smaller indirect associations primarily through microbial pathways. These findings indicate that differences in SOC pools across carbonate lithologies are better explained by contrasting biological and mineral environments than by calcium properties alone. By separating SOC into POC and MAOC and

integrating microbial, mineral-associated, and calcium-related processes, this study clarifies the fraction-specific pathways associated with carbon storage in karst soils and highlights the value of representing these pathways separately in conceptual and process-based models of carbonate-soil C cycling. Future research combining microbial biomarkers, isotope tracing, and direct characterization of organo-mineral and Ca–organic associations could further resolve the mechanisms underlying these patterns.

Declarations

Competing interests

The authors have no relevant financial or non-financial interests to disclose.

Funding

This study was supported by the National Key Research and Development Plan (Grant No. 2023YFF0806002), the National Natural Science Foundation of China (Grant No. 42371039), and the Strategic Priority Research Program of the Chinese Academy of Sciences (Grant No. XDA23040202).

Author Contribution

M M I: Conceptualization, methodology, investigation, formal analysis, data curation, software, writing – original draft. C L: Conceptualization, Methodology, writing – review and editing, Conceptualization. J C: Funding acquisition, writing – review and editing. J W: writing – review. M L: Investigation. J Z: Investigation. W T: Investigation. J T: Conceptualization, funding acquisition, and editing.

Data Availability

Data supporting the findings of this study are presented in the article and its supplementary materials. The underlying raw data are available from the corresponding author on reasonable request. The dataset forms part of an ongoing thesis research project and is currently being used for related analyses.

References

1. Barré P, Quénéa K, Vidal A et al (2018) Microbial and plant-derived compounds both contribute to persistent soil organic carbon in temperate soils. Biogeochemistry 140:81–92. https://doi.org/10.1007/s10533-018-0475-5
2. Chen H, Li D, Mao Q et al (2019a) Resource limitation of soil microbes in karst ecosystems. Sci Total Environ 650:241–248. https://doi.org/10.1016/j.scitotenv.2018.09.036

3. Chen H, Li D, Xiao K, Wang K (2018) Soil microbial processes and resource limitation in karst and non-karst forests. Funct Ecol 32:1400–1409. https://doi.org/10.1111/1365-2435.13069
4. Chen L, Liu L, Qin S et al (2019b) Regulation of priming effect by soil organic matter stability over a broad geographic scale. Nat Commun 10:5112. https://doi.org/10.1038/s41467-019-13119-z
5. Cotrufo MF, Ranalli MG, Haddix ML et al (2019) Soil carbon storage informed by particulate and mineral-associated organic matter. Nat Geosci 12:989–994. https://doi.org/10.1038/s41561-019-0484-6
6. Cotrufo MF, Wallenstein MD, Boot CM et al (2013) The Microbial Efficiency-Matrix Stabilization (MEMS) framework integrates plant litter decomposition with soil organic matter stabilization: do labile plant inputs form stable soil organic matter? Glob Change Biol 19:988–995. https://doi.org/10.1111/gcb.12113
7. Danks NP, Sharma PN, Sarstedt M (2020) Model selection uncertainty and multimodel inference in partial least squares structural equation modeling (PLS-SEM). J Bus Res 113:13–24. https://doi.org/10.1016/j.jbusres.2020.03.019
8. Dou X, Zhang C, Zhang J et al (2024) Relationship between calcium forms and organic carbon content in aggregates of calcareous soils in northern China. Soil Tillage Res 244:106210. https://doi.org/10.1016/j.still.2024.106210
9. Dou X, Zhang J, Zhang C et al (2023) Calcium carbonate regulates soil organic carbon accumulation by mediating microbial communities in northern China. CATENA 231:107327. https://doi.org/10.1016/j.catena.2023.107327
10. Elith J, Leathwick JR, Hastie T (2008) A working guide to boosted regression trees. J Anim Ecol 77:802–813. https://doi.org/10.1111/j.1365-2656.2008.01390.x
11. Fierer N, Schimel JP, Holden PA (2003) Variations in microbial community composition through two soil depth profiles. Soil Biol Biochem 35:167–176. https://doi.org/10.1016/S0038-0717(02)00251-1
12. Frostegård Å, Bååth E, Tunlio A (1993) Shifts in the structure of soil microbial communities in limed forests as revealed by phospholipid fatty acid analysis. Soil Biol Biochem 25:723–730. https://doi.org/10.1016/0038-0717(93)90113-P
13. Georgiou K, Jackson RB, Vindušková O et al (2022) Global stocks and capacity of mineral-associated soil organic carbon. Nat Commun 13:3797. https://doi.org/10.1038/s41467-022-31540-9
14. Guo Z, Zhang X, Dungait JAJ et al (2021) Contribution of soil microbial necromass to SOC stocks during vegetation recovery in a subtropical karst ecosystem. Sci Total Environ 761:143945. https://doi.org/10.1016/j.scitotenv.2020.143945
15. Haddix ML, Gregorich EG, Helgason BL et al (2020) Climate, carbon content, and soil texture control the independent formation and persistence of particulate and mineral-associated organic matter in soil. Geoderma 363:114160. https://doi.org/10.1016/j.geoderma.2019.114160
16. Hu L, Li Q, Yan J et al (2022a) Vegetation restoration facilitates belowground microbial network complexity and recalcitrant soil organic carbon storage in southwest China karst region. Sci Total

Environ 820:153137. https://doi.org/10.1016/j.scitotenv.2022.153137

17. Hu P, Zhang W, Chen H et al (2022b) Lithologic control of microbial-derived carbon in forest soils. Soil Biol Biochem 167:108600. https://doi.org/10.1016/j.soilbio.2022.108600
18. Hu P, Zhang W, Kuzyakov Y et al (2023) Linking bacterial life strategies with soil organic matter accrual by karst vegetation restoration. Soil Biol Biochem 177:108925. https://doi.org/10.1016/j.soilbio.2022.108925
19. Hu P, Zhang W, Nottingham AT et al (2024) Lithological Controls on Soil Aggregates and Minerals Regulate Microbial Carbon Use Efficiency and Necromass Stability. Environ Sci Technol 58:21186–21199. https://doi.org/10.1021/acs.est.4c07264
20. Kallenbach CM, Frey SD, Grandy AS (2016) Direct evidence for microbial-derived soil organic matter formation and its ecophysiological controls. Nat Commun 7:13630. https://doi.org/10.1038/ncomms13630
21. Kleber M, Eusterhues K, Keiluweit M et al (2015) Mineral–Organic Associations: Formation, Properties, and Relevance in Soil Environments. In: Advances in Agronomy. Elsevier, pp 1–140
22. Kögel-Knabner I, Guggenberger G, Kleber M et al (2008) Organo-mineral associations in temperate soils: Integrating biology, mineralogy, and organic matter chemistry. J Plant Nutr Soil Sci 171:61–82. https://doi.org/10.1002/jpln.200700048
23. Lan J, Jiang Y, Huang M (2025) Vegetation restoration enhances soil organic carbon accumulation in Southwest China's karst region: The role of aggregation, calcium, and microbes. CATENA 257:109184. https://doi.org/10.1016/j.catena.2025.109184
24. Lavallee JM, Soong JL, Cotrufo MF (2020) Conceptualizing soil organic matter into particulate and mineral-associated forms to address global change in the 21st century. Glob Change Biol 26:261–273. https://doi.org/10.1111/gcb.14859
25. Li C, Cui J, Wang T et al (2026) Synergistic mineral-microbial regulation dominates mineral-associated organic carbon accrual by carbonate weathering. CATENA 270:110174. https://doi.org/10.1016/j.catena.2026.110174
26. Liang C, Amelung W, Lehmann J, Kästner M (2019) Quantitative assessment of microbial necromass contribution to soil organic matter. Glob Change Biol 25:3578–3590. https://doi.org/10.1111/gcb.14781
27. Liang C, Schimel JP, Jastrow JD (2017) The importance of anabolism in microbial control over soil carbon storage. Nat Microbiol 2:17105. https://doi.org/10.1038/nmicrobiol.2017.105
28. Lin Q, Chen S, Feng X et al (2025) Lithological impact on topsoil organic carbon storage of karst forest soils shaped by aggregate pool complexity and their molecular composition. Appl Soil Ecol 206:105800. https://doi.org/10.1016/j.apsoil.2024.105800
29. Liu S, Zhang W, Wang K et al (2015) Factors controlling accumulation of soil organic carbon along vegetation succession in a typical karst region in Southwest China. Sci Total Environ 521–522:52–58. https://doi.org/10.1016/j.scitotenv.2015.03.074

30. Lu R (2000) Analytical Methods of Soil Agrochemistry. China Agricultural Science and Technology Publishing House, Beijing, China
31. Mikutta R, Kleber M, Torn MS, Jahn R (2006) Stabilization of soil organic matter: association with minerals or chemical recalcitrance? Biogeochemistry 77:25–56
32. Poeplau C, Don A, Six J et al (2018) Isolating organic carbon fractions with varying turnover rates in temperate agricultural soils – A comprehensive method comparison. Soil Biol Biochem 125:10–26. https://doi.org/10.1016/j.soilbio.2018.06.025
33. Rasmussen C, Heckman K, Wieder WR et al (2018) Beyond clay: towards an improved set of variables for predicting soil organic matter content. Biogeochemistry 137:297–306. https://doi.org/10.1007/s10533-018-0424-3
34. Rowley MC, Grand S, Spangenberg JE, Verrecchia EP (2021) Evidence linking calcium to increased organo-mineral association in soils. Biogeochemistry 153:223–241. https://doi.org/10.1007/s10533-021-00779-7
35. Rowley MC, Grand S, Verrecchia ÉP (2018) Calcium-mediated stabilisation of soil organic carbon. Biogeochemistry 137:27–49. https://doi.org/10.1007/s10533-017-0410-1
36. Schmidt MW, Torn MS, Abiven S et al (2011) Persistence of soil organic matter as an ecosystem property. Nature 478:49–56
37. Shabtai IA, Wilhelm RC, Schweizer SA et al (2023) Calcium promotes persistent soil organic matter by altering microbial transformation of plant litter. Nat Commun 14:6609. https://doi.org/10.1038/s41467-023-42291-6
38. Six J, Conant RT, Paul EA, Paustian K (2002) Stabilization mechanisms of soil organic matter: implications for C-saturation of soils. Plant Soil 241:155–176
39. Sokol NW, Bradford MA (2019) Microbial formation of stable soil carbon is more efficient from belowground than aboveground input. Nat Geosci 12:46–53. https://doi.org/10.1038/s41561-018-0258-6
40. Sokol NW, Sanderman J, Bradford MA (2019) Pathways of mineral-associated soil organic matter formation: Integrating the role of plant carbon source, chemistry, and point of entry. Glob Change Biol 25:12–24. https://doi.org/10.1111/gcb.14482
41. Sokol NW, Slessarev E, Marschmann GL et al (2022) Life and death in the soil microbiome: how ecological processes influence biogeochemistry. Nat Rev Microbiol 20:415–430. https://doi.org/10.1038/s41579-022-00695-z
42. Solly EF, Weber V, Zimmermann S et al (2020) A Critical Evaluation of the Relationship Between the Effective Cation Exchange Capacity and Soil Organic Carbon Content in Swiss Forest Soils. https://doi.org/10.3389/ffgc.2020.00098. Front For Glob Change 3:
43. Tang T, Hu P, Zhang W et al (2023) The Role of Bedrock Geochemistry and Climate in Soil Organic Matter Stability in Subtropical Karst Forests of Southwest China. Forests 14:1467. https://doi.org/10.3390/f14071467

44. Tao F, Huang Y, Hungate BA et al (2023) Microbial carbon use efficiency promotes global soil carbon storage. Nature 618:981–985. https://doi.org/10.1038/s41586-023-06042-3
45. Varga T, Kukkadapu RK, Kovarik L et al (2025) The role of Ca-bridged organic matter in an alkaline soil, as revealed by multimodal chemical imaging. Geoderma 456:117256. https://doi.org/10.1016/j.geoderma.2025.117256
46. Wagai R, Mayer LM (2007) Sorptive stabilization of organic matter in soils by hydrous iron oxides. Geochim Cosmochim Acta 71:25–35. https://doi.org/10.1016/j.gca.2006.08.047
47. Wang B, An S, Liang C et al (2021a) Microbial necromass as the source of soil organic carbon in global ecosystems. Soil Biol Biochem 162:108422. https://doi.org/10.1016/j.soilbio.2021.108422
48. Wang K, Zhang C, Chen H et al (2019) Karst landscapes of China: patterns, ecosystem processes and services. Landsc Ecol 34:2743–2763. https://doi.org/10.1007/s10980-019-00912-w
49. Wang M, Chen H, Zhang W, Wang K (2018) Soil nutrients and stoichiometric ratios as affected by land use and lithology at county scale in a karst area, southwest China. Sci Total Environ 619–620:1299–1307. https://doi.org/10.1016/j.scitotenv.2017.11.175
50. Wang S, Jia Y, Liu T et al (2021b) Delineating the Role of Calcium in the Large-Scale Distribution of Metal-Bound Organic Carbon in Soils. Geophys Res Lett 48. https://doi.org/10.1029/2021GL092391. e2021GL092391
51. Wen L, Li D, Chen H, Wang K (2017) Dynamics of soil organic carbon in density fractions during post-agricultural succession over two lithology types, southwest China. J Environ Manage 201:199–206. https://doi.org/10.1016/j.jenvman.2017.06.048
52. Witzgall K, Vidal A, Schubert DI et al (2021) Particulate organic matter as a functional soil component for persistent soil organic carbon. Nat Commun 12:4115. https://doi.org/10.1038/s41467-021-24192-8
53. Xiao S, Chen W, Zhang W et al (2026) Vegetation restoration is associated with soil microbial community reassembly and necromass carbon accumulation via calcium mediation in a degraded karst ecosystem. CATENA 272:110353. https://doi.org/10.1016/j.catena.2026.110353
54. Xie L, Hu P, Ling Q et al (2024) Effects of soil aggregates and minerals on microbial necromass carbon are regulated by parent materials. Appl Soil Ecol 200:105431. https://doi.org/10.1016/j.apsoil.2024.105431
55. Xuan M, Ai L, Wu F et al (2024) Biomarkers evidence shows a preferential occlusion of microbial necromass in mineral-associated and not particle organic matter. Geoderma 450:117030. https://doi.org/10.1016/j.geoderma.2024.117030
56. Yang Y, Gunina A, Cheng H et al (2025) Unlocking Mechanisms for Soil Organic Matter Accumulation: Carbon Use Efficiency and Microbial Necromass as the Keys. Glob Change Biol 31:e70033. https://doi.org/10.1111/gcb.70033
57. Zhou Z, Ren C, Wang C et al (2024) Global turnover of soil mineral-associated and particulate organic carbon. Nat Commun 15:5329. https://doi.org/10.1038/s41467-024-49743-7

58. Zhu E, Liu Z, Ma L et al (2024) Enhanced Mineral Preservation Rather Than Microbial Residue Production Dictates the Accrual of Mineral-Associated Organic Carbon Along a Weathering Gradient. Geophys Res Lett 51:e2024GL108466. https://doi.org/10.1029/2024GL108466
59. Zhu Z, Xiao K, Liu Y et al (2026) Microbial necromass dominates particulate and mineral-associated organic carbon accumulation in calcareous soil following afforestation. J Appl Ecol 63:e70364. https://doi.org/10.1111/1365-2664.70364

Figures

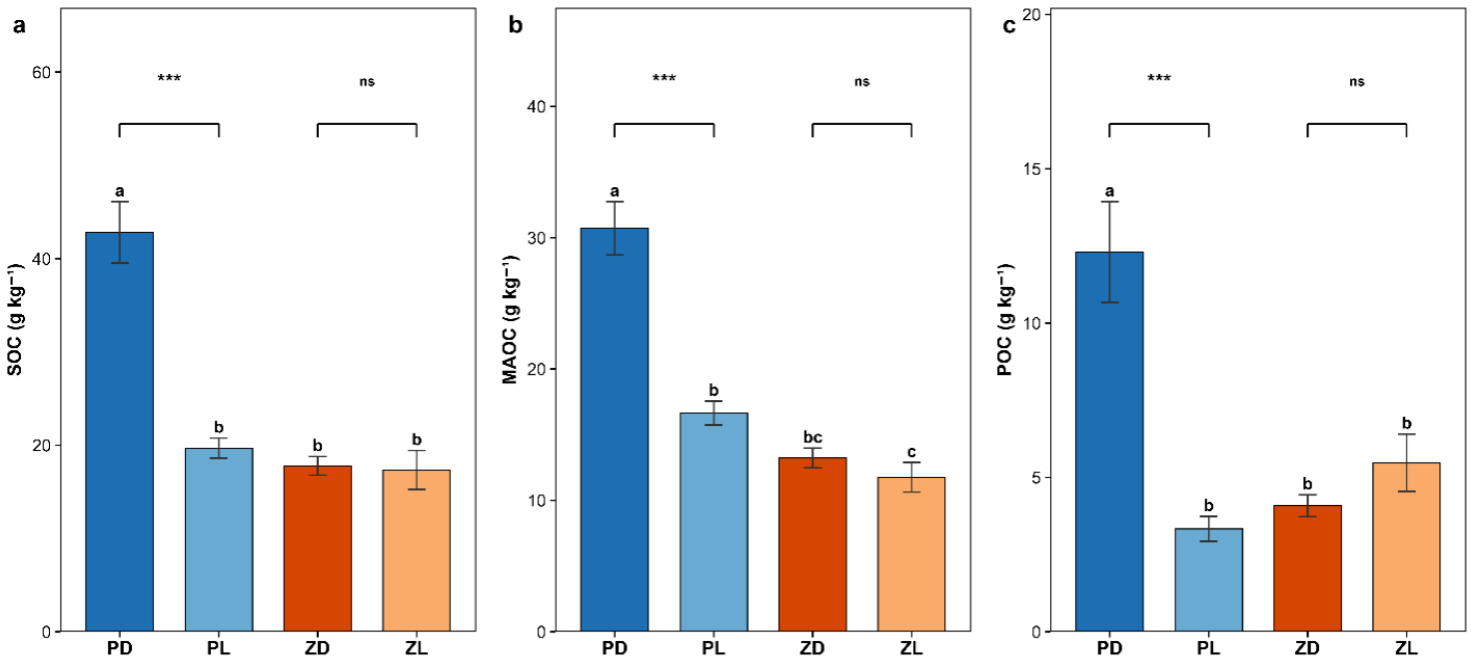


Figure 1

(a) Soil organic carbon (SOC), (b) mineral-associated organic carbon (MAOC), and (c) particulate organic carbon (POC) concentrations across four site–lithology treatments (PD, Puding Dolomite; PL, Puding Limestone; ZD, Zunyi Dolomite; ZL, Zunyi Limestone; n = 9 per treatment, slope positions pooled). Bars represent mean ± SE. Different lowercase letters indicate significant differences among treatments ($p < 0.05$, LSD test). Asterisks above horizontal brackets denote significant differences between Dolomite and Limestone within the same site based on independent-samples t-test (*$p < 0.05$; **$p < 0.01$; ***$p < 0.001$; ns, not significant).

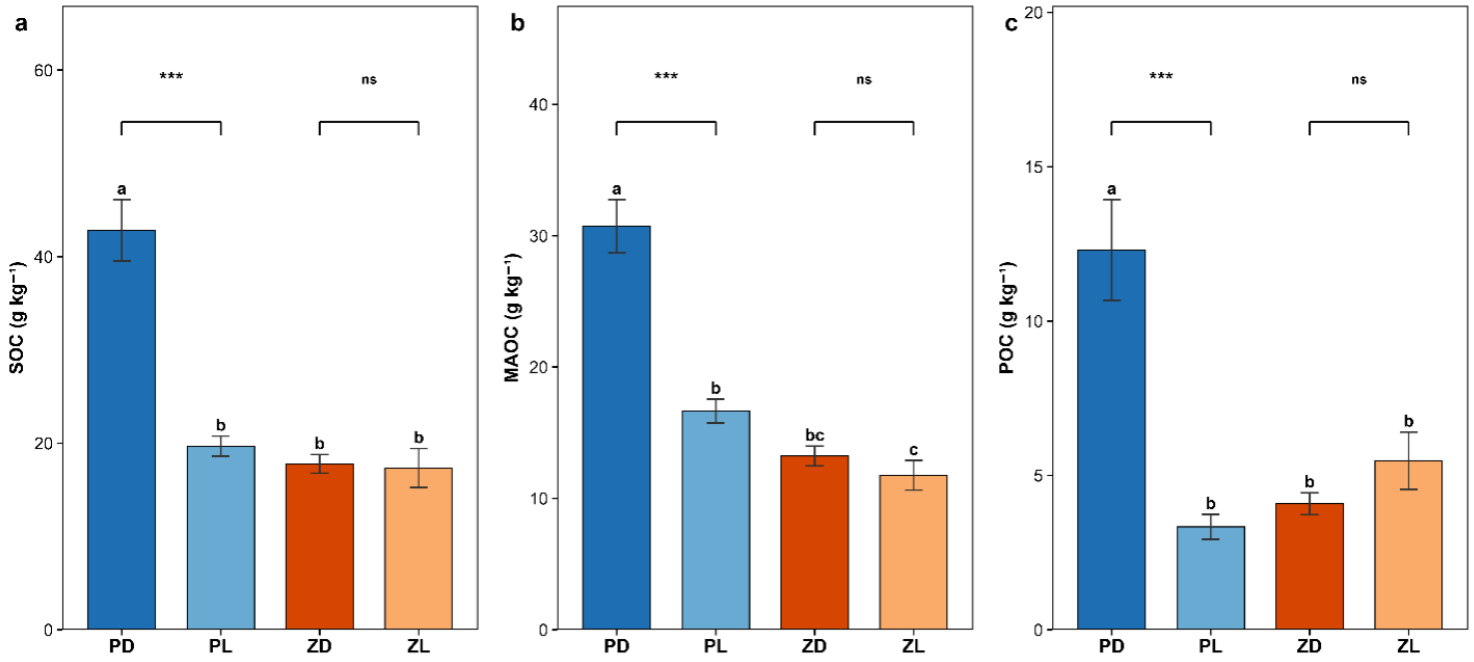


Figure 1

(a) Soil organic carbon (SOC), (b) mineral-associated organic carbon (MAOC), and (c) particulate organic carbon (POC) concentrations across four site–lithology treatments (PD, Puding Dolomite; PL, Puding Limestone; ZD, Zunyi Dolomite; ZL, Zunyi Limestone; n = 9 per treatment, slope positions pooled). Bars represent mean ± SE. Different lowercase letters indicate significant differences among treatments ($p < 0.05$, LSD test). Asterisks above horizontal brackets denote significant differences between Dolomite and Limestone within the same site based on independent-samples t-test (*$p < 0.05$; **$p < 0.01$; ***$p < 0.001$; ns, not significant).

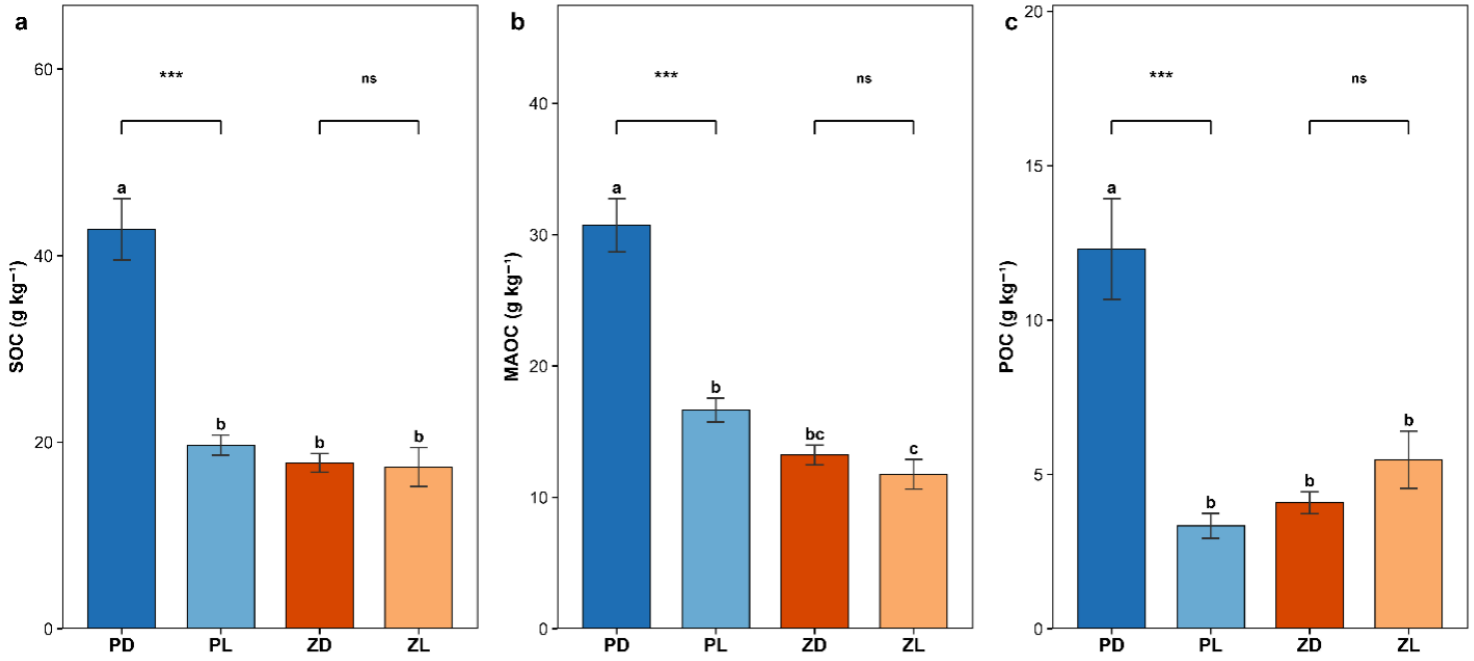


Figure 1

(a) Soil organic carbon (SOC), (b) mineral-associated organic carbon (MAOC), and (c) particulate organic carbon (POC) concentrations across four site–lithology treatments (PD, Puding Dolomite; PL, Puding Limestone; ZD, Zunyi Dolomite; ZL, Zunyi Limestone; n = 9 per treatment, slope positions pooled). Bars represent mean ± SE. Different lowercase letters indicate significant differences among treatments ($p < 0.05$, LSD test). Asterisks above horizontal brackets denote significant differences between Dolomite and Limestone within the same site based on independent-samples t-test (*$p < 0.05$; **$p < 0.01$; ***$p < 0.001$; ns, not significant).

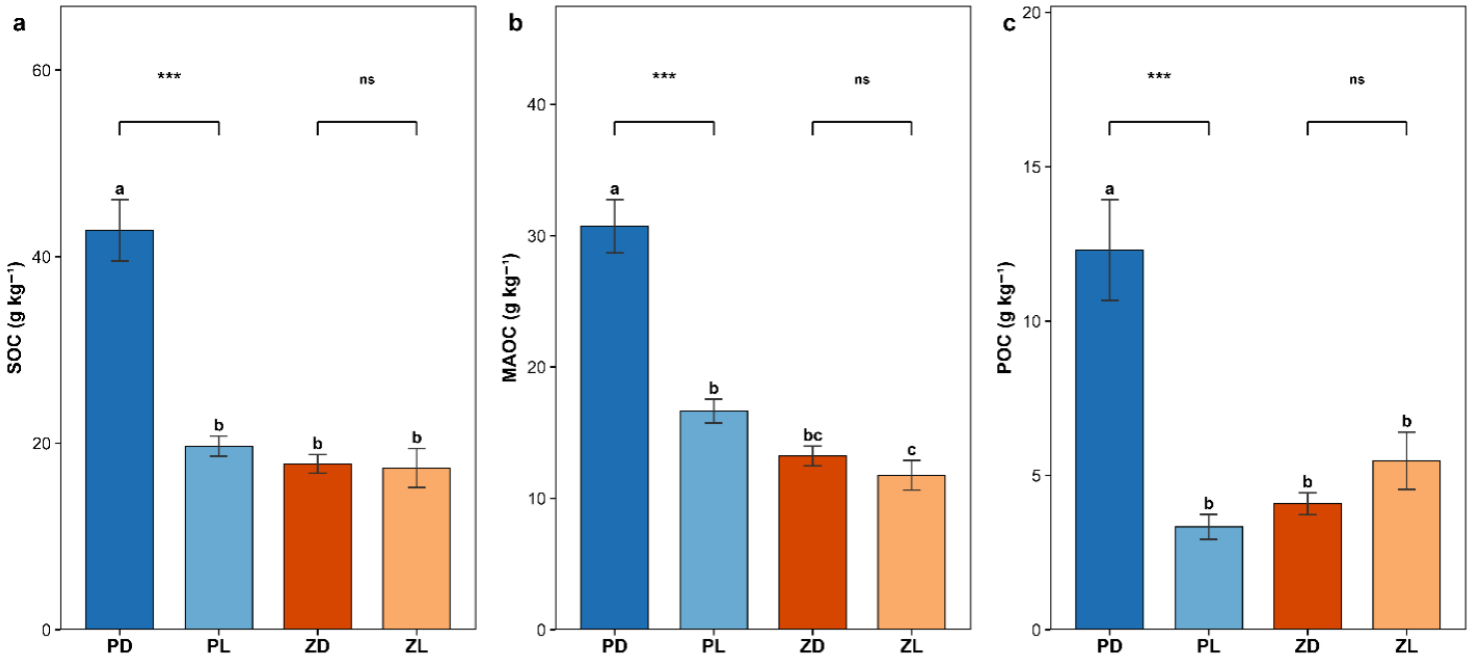


Figure 1

(a) Soil organic carbon (SOC), (b) mineral-associated organic carbon (MAOC), and (c) particulate organic carbon (POC) concentrations across four site–lithology treatments (PD, Puding Dolomite; PL, Puding Limestone; ZD, Zunyi Dolomite; ZL, Zunyi Limestone; n = 9 per treatment, slope positions pooled). Bars represent mean ± SE. Different lowercase letters indicate significant differences among treatments ($p < 0.05$, LSD test). Asterisks above horizontal brackets denote significant differences between Dolomite and Limestone within the same site based on independent-samples t-test (*$p < 0.05$; **$p < 0.01$; ***$p < 0.001$; ns, not significant).

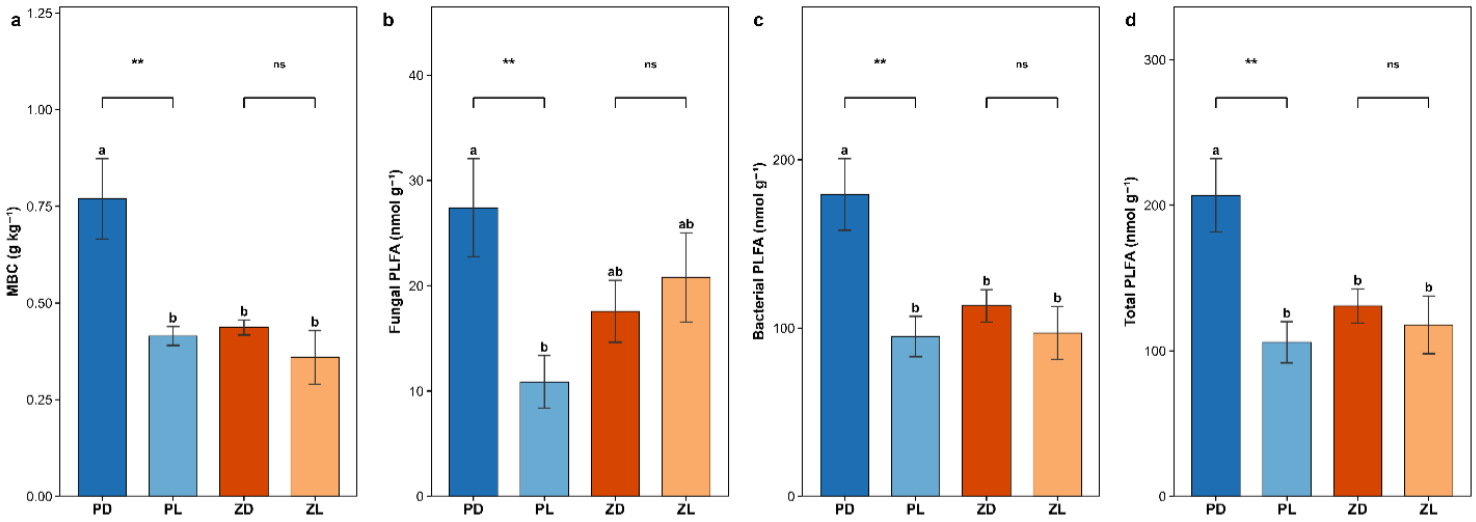


Figure 2

Microbial properties across the four site–lithology treatments (n = 9 per treatment): (a) microbial biomass carbon (MBC), (b) fungal phospholipid fatty acid (FunPLFA), (c) bacterial phospholipid fatty acid (BacPLFA), and (d) total phospholipid fatty acid (TotalPLFA). Bars represent mean ± SE. Different lowercase letters indicate significant differences among treatments ($p < 0.05$, LSD test). Asterisks denote significant differences between Dolomite and Limestone within the same site (independent-samples t-test; *$p < 0.05$; **$p < 0.01$; ***$p < 0.001$; ns, not significant).

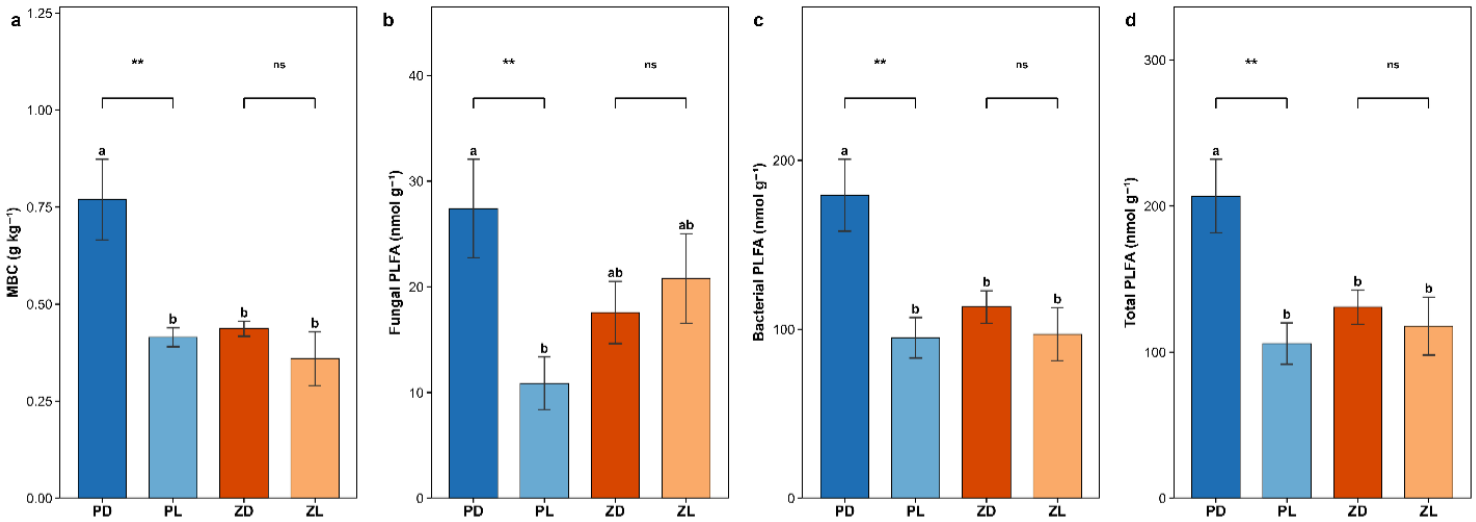


Figure 2

Microbial properties across the four site–lithology treatments (n = 9 per treatment): (a) microbial biomass carbon (MBC), (b) fungal phospholipid fatty acid (FunPLFA), (c) bacterial phospholipid fatty acid (BacPLFA), and (d) total phospholipid fatty acid (TotalPLFA). Bars represent mean ± SE. Different lowercase letters indicate significant differences among treatments ($p < 0.05$, LSD test). Asterisks denote significant differences between Dolomite and Limestone within the same site (independent-samples t-test; *$p < 0.05$; **$p < 0.01$; ***$p < 0.001$; ns, not significant).

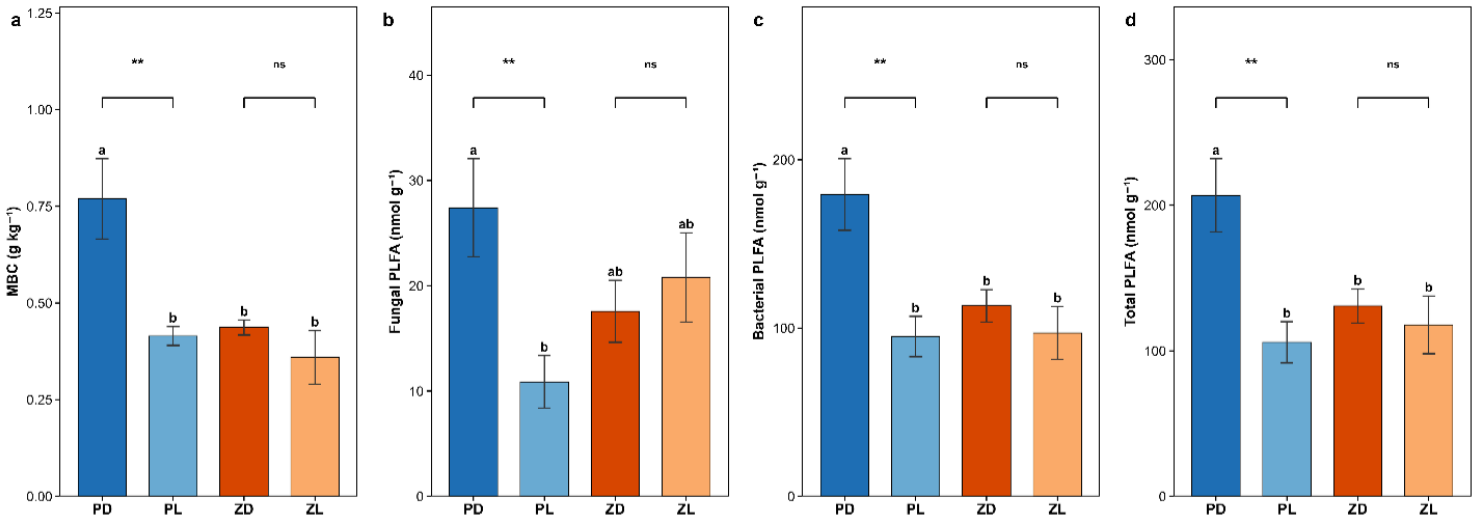


Figure 2

Microbial properties across the four site–lithology treatments (n = 9 per treatment): (a) microbial biomass carbon (MBC), (b) fungal phospholipid fatty acid (FunPLFA), (c) bacterial phospholipid fatty acid (BacPLFA), and (d) total phospholipid fatty acid (TotalPLFA). Bars represent mean ± SE. Different lowercase letters indicate significant differences among treatments ($p < 0.05$, LSD test). Asterisks denote significant differences between Dolomite and Limestone within the same site (independent-samples t-test; *$p < 0.05$; **$p < 0.01$; ***$p < 0.001$; ns, not significant).

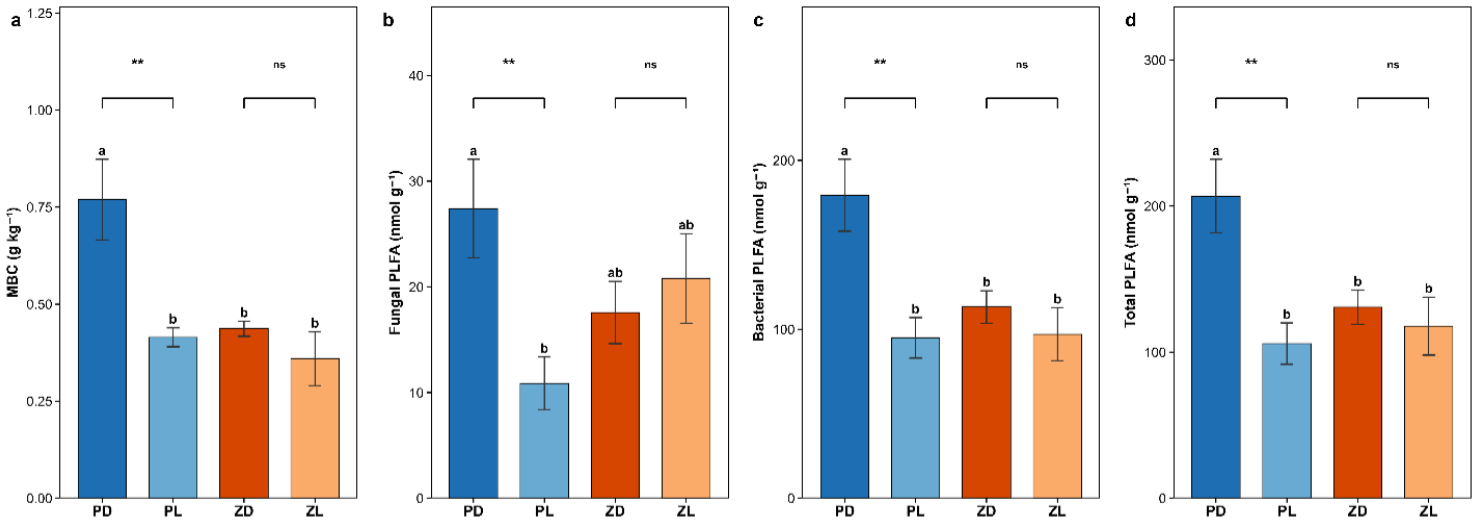


Figure 2

Microbial properties across the four site–lithology treatments (n = 9 per treatment): (a) microbial biomass carbon (MBC), (b) fungal phospholipid fatty acid (FunPLFA), (c) bacterial phospholipid fatty acid (BacPLFA), and (d) total phospholipid fatty acid (TotalPLFA). Bars represent mean ± SE. Different lowercase letters indicate significant differences among treatments ($p < 0.05$, LSD test). Asterisks denote significant differences between Dolomite and Limestone within the same site (independent-samples t-test; *$p < 0.05$; **$p < 0.01$; ***$p < 0.001$; ns, not significant).

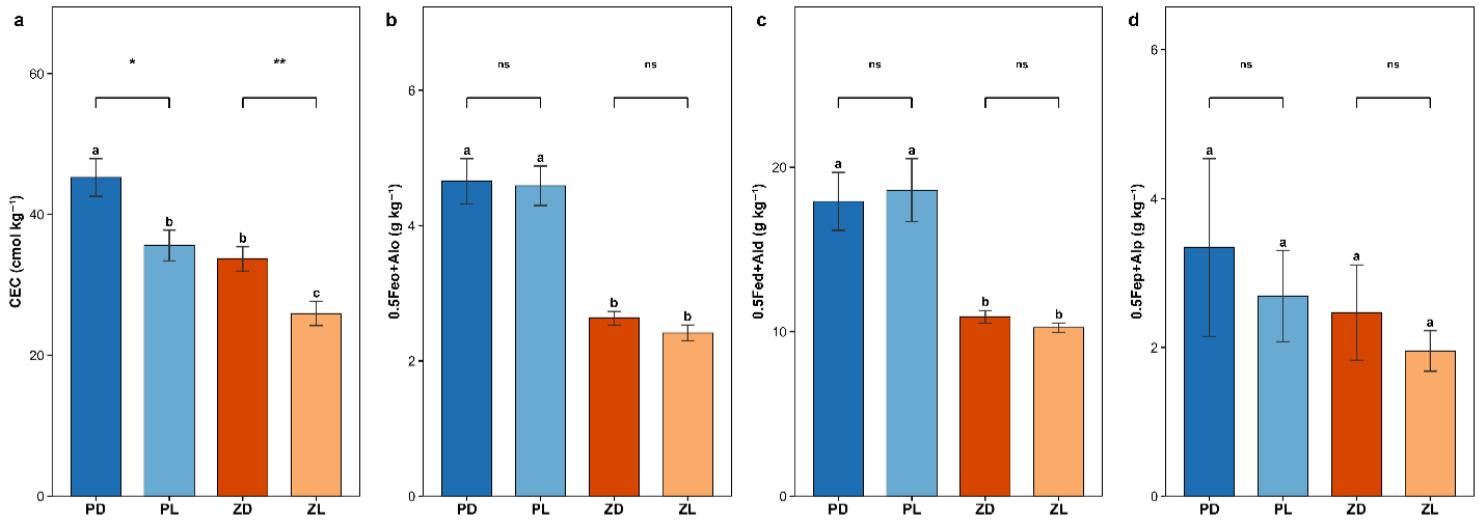


Figure 3

Mineral properties across the four site–lithology treatments (n = 9 per treatment): (a) cation exchange capacity (CEC), (b) oxalate-extractable Fe–Al (0.5Feo+Alo), (c) dithionite-extractable Fe–Al (0.5Fed+Ald), and (d) pyrophosphate-extractable Fe–Al (0.5Fep+Alp). Bars represent mean ± SE. Different lowercase letters indicate significant differences among treatments ($p < 0.05$, LSD test). Asterisks denote significant differences between Dolomite and Limestone within the same site (independent-samples t-test; *$p < 0.05$; **$p < 0.01$; ***$p < 0.001$; ns, not significant).

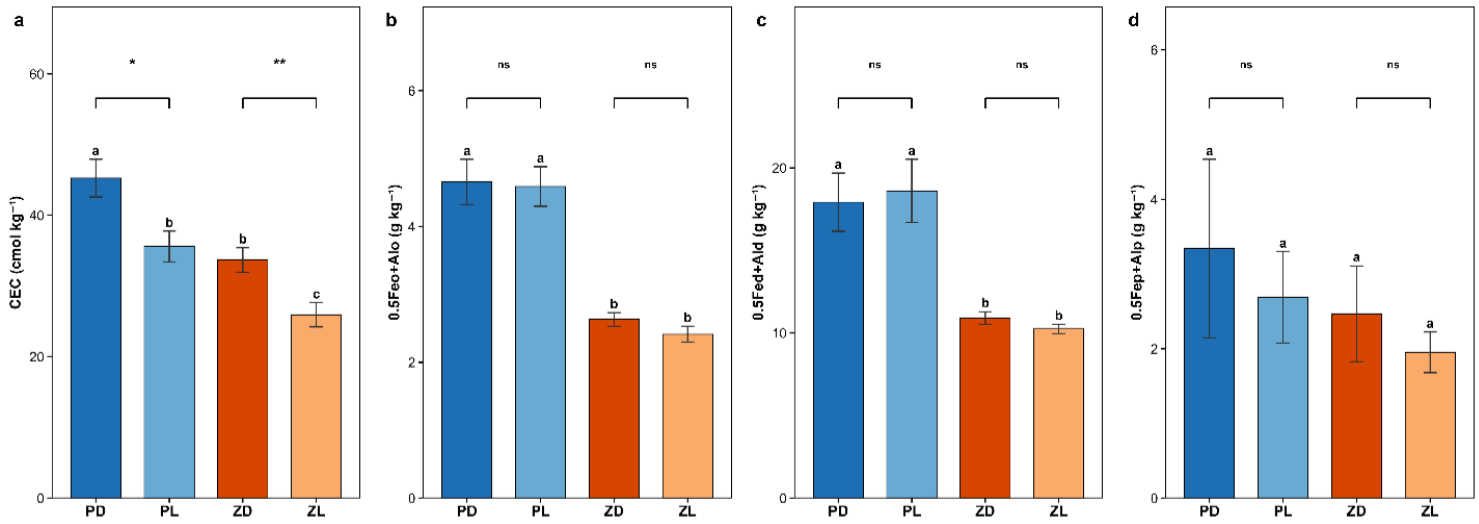


Figure 3

Mineral properties across the four site–lithology treatments (n = 9 per treatment): (a) cation exchange capacity (CEC), (b) oxalate-extractable Fe–Al (0.5Feo+Alo), (c) dithionite-extractable Fe–Al (0.5Fed+Ald), and (d) pyrophosphate-extractable Fe–Al (0.5Fep+Alp). Bars represent mean ± SE. Different lowercase letters indicate significant differences among treatments ($p < 0.05$, LSD test). Asterisks denote significant differences between Dolomite and Limestone within the same site (independent-samples t-test; *$p < 0.05$; **$p < 0.01$; ***$p < 0.001$; ns, not significant).

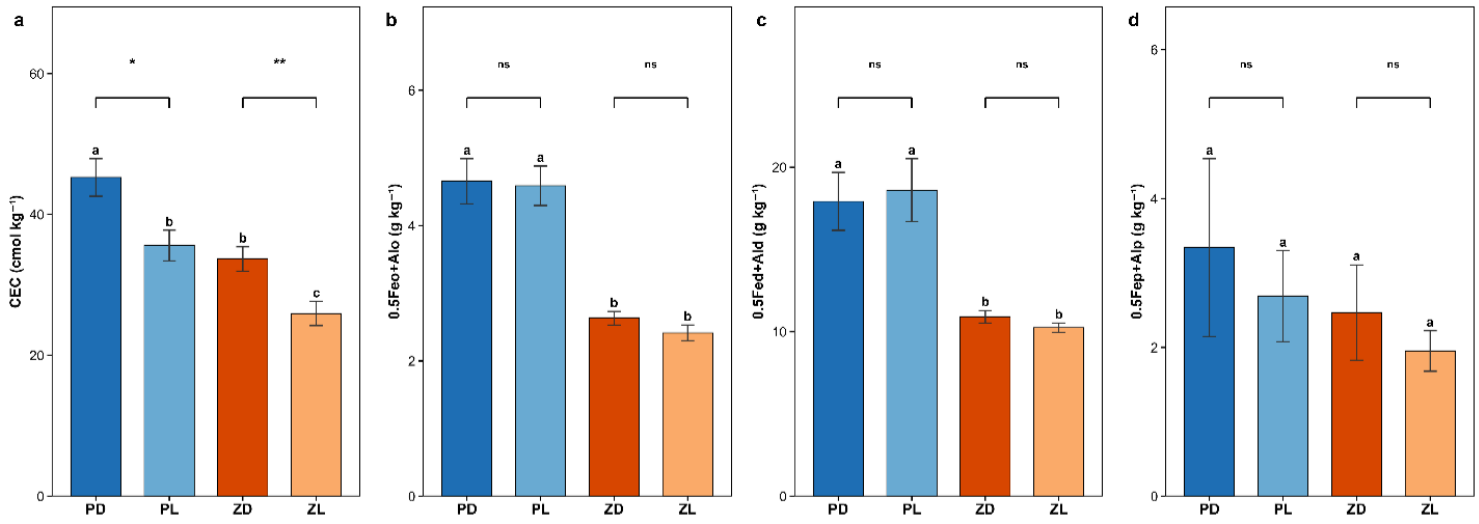


Figure 3

Mineral properties across the four site–lithology treatments (n = 9 per treatment): (a) cation exchange capacity (CEC), (b) oxalate-extractable Fe–Al (0.5Feo+Alo), (c) dithionite-extractable Fe–Al (0.5Fed+Ald), and (d) pyrophosphate-extractable Fe–Al (0.5Fep+Alp). Bars represent mean ± SE. Different lowercase letters indicate significant differences among treatments ($p < 0.05$, LSD test). Asterisks denote significant differences between Dolomite and Limestone within the same site (independent-samples t-test; *$p < 0.05$; **$p < 0.01$; ***$p < 0.001$; ns, not significant).

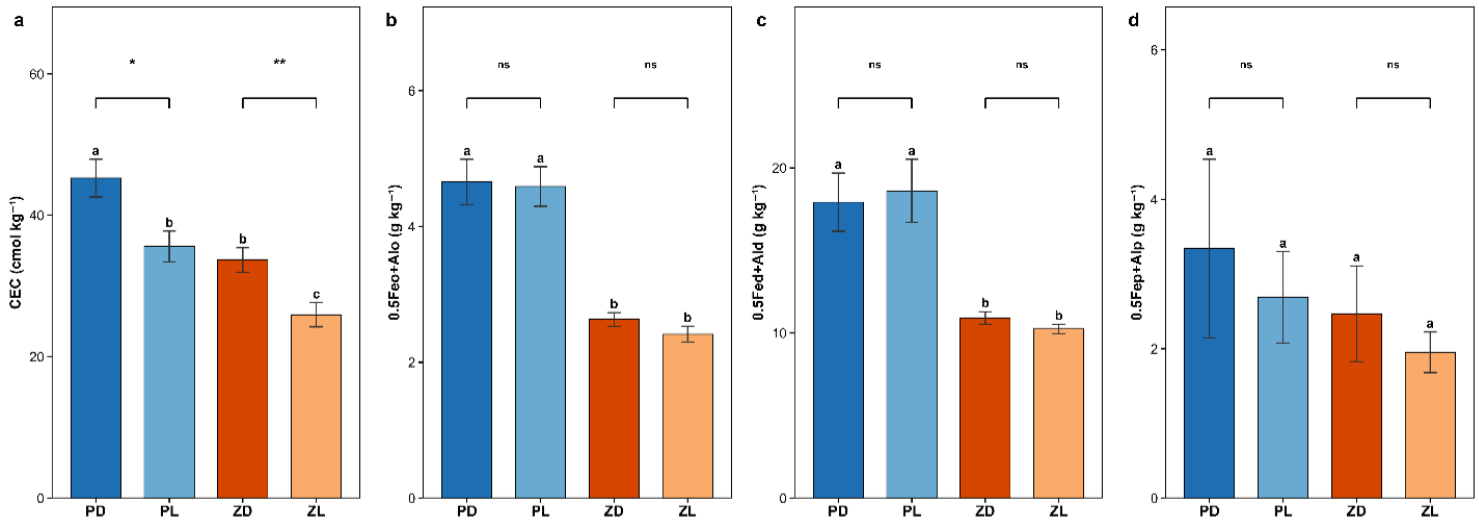


Figure 3

Mineral properties across the four site–lithology treatments (n = 9 per treatment): (a) cation exchange capacity (CEC), (b) oxalate-extractable Fe–Al (0.5Feo+Alo), (c) dithionite-extractable Fe–Al (0.5Fed+Ald), and (d) pyrophosphate-extractable Fe–Al (0.5Fep+Alp). Bars represent mean ± SE. Different lowercase letters indicate significant differences among treatments ($p < 0.05$, LSD test). Asterisks denote significant differences between Dolomite and Limestone within the same site (independent-samples t-test; *$p < 0.05$; **$p < 0.01$; ***$p < 0.001$; ns, not significant).

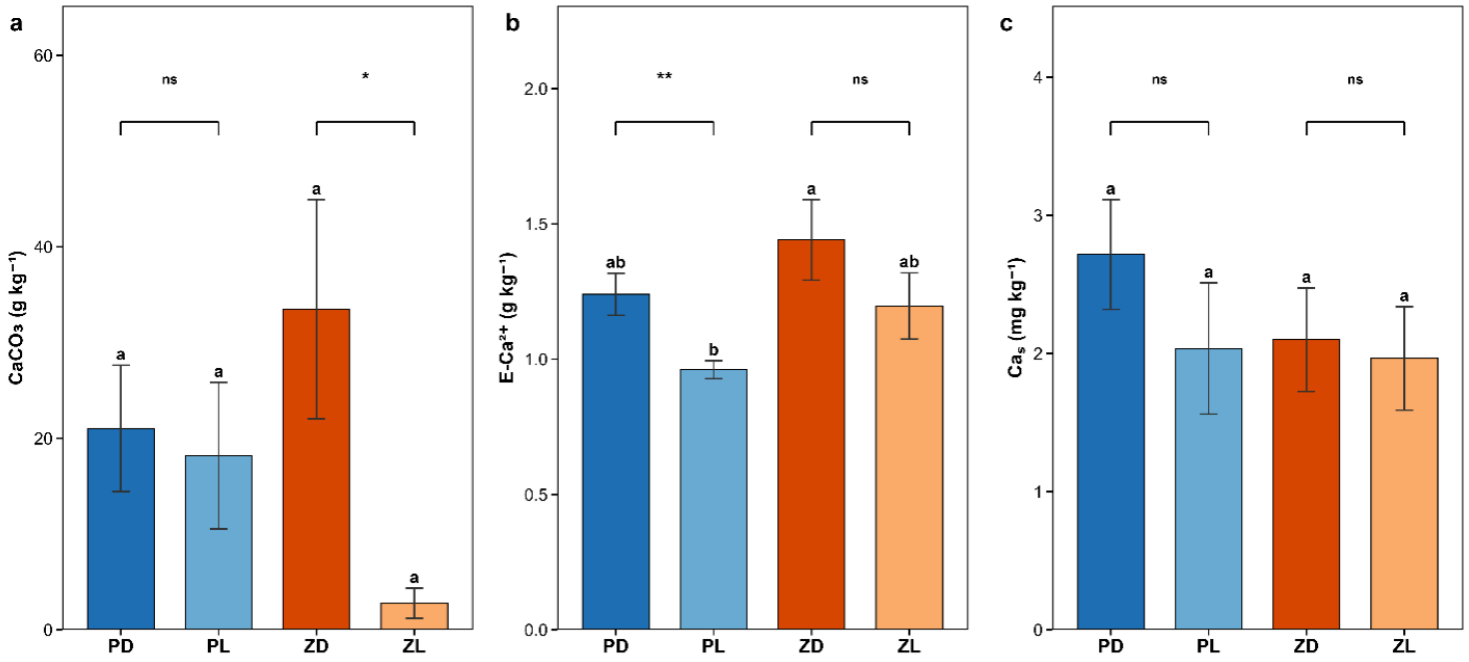


Figure 4

Calcium fractions across the four site–lithology treatments (n = 9 per treatment): (a) calcium carbonate ($CaCO_3$), (b) exchangeable Ca^{2+} (E-Ca^{2+}), and (c) sulfate-extractable Ca (Ca□). Bars represent mean ± SE. Different lowercase letters indicate significant differences among treatments ($p < 0.05$, LSD test). Asterisks denote significant differences between Dolomite and Limestone within the same site (independent-samples t-test; *$p < 0.05$; **$p < 0.01$; ***$p < 0.001$; ns, not significant).

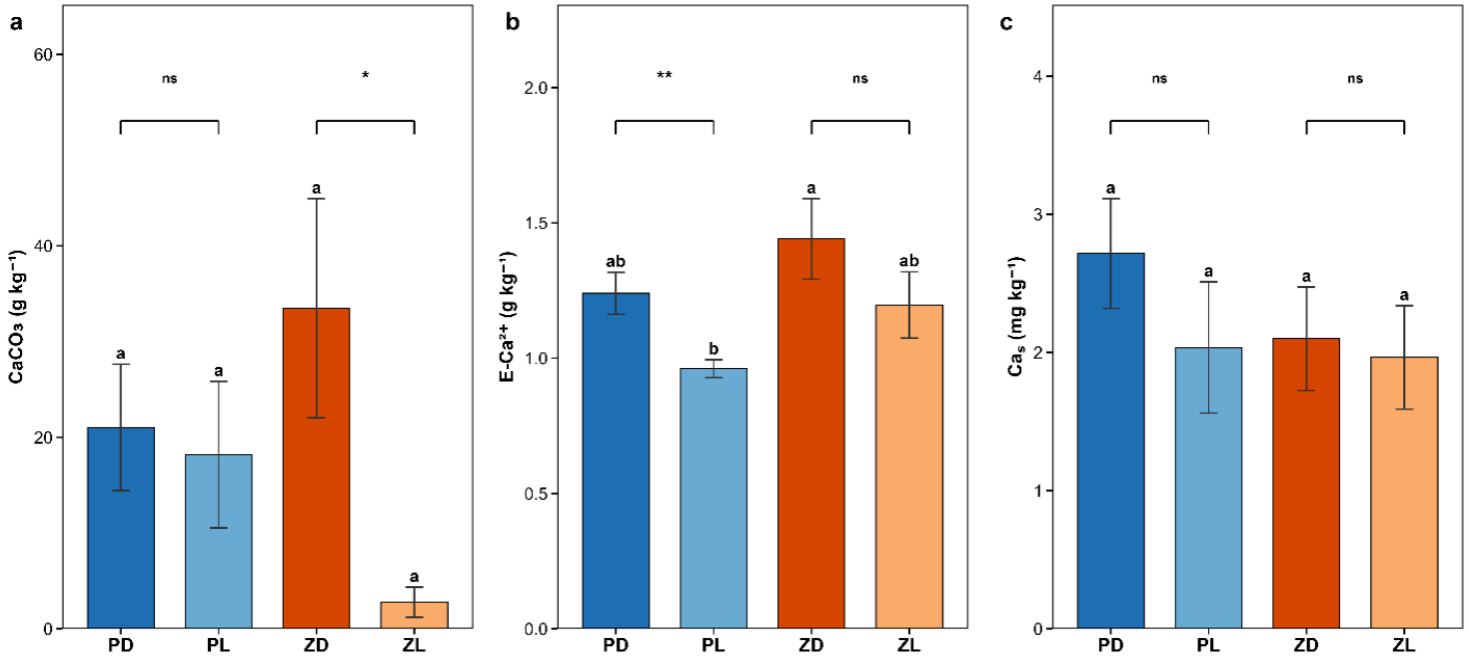


Figure 4

Calcium fractions across the four site–lithology treatments (n = 9 per treatment): (a) calcium carbonate ($CaCO_3$), (b) exchangeable Ca^{2+} (E-Ca^{2+}), and (c) sulfate-extractable Ca (Ca□). Bars represent mean ± SE. Different lowercase letters indicate significant differences among treatments ($p < 0.05$, LSD test). Asterisks denote significant differences between Dolomite and Limestone within the same site (independent-samples t-test; *p < 0.05; **p < 0.01; ***p < 0.001; ns, not significant).

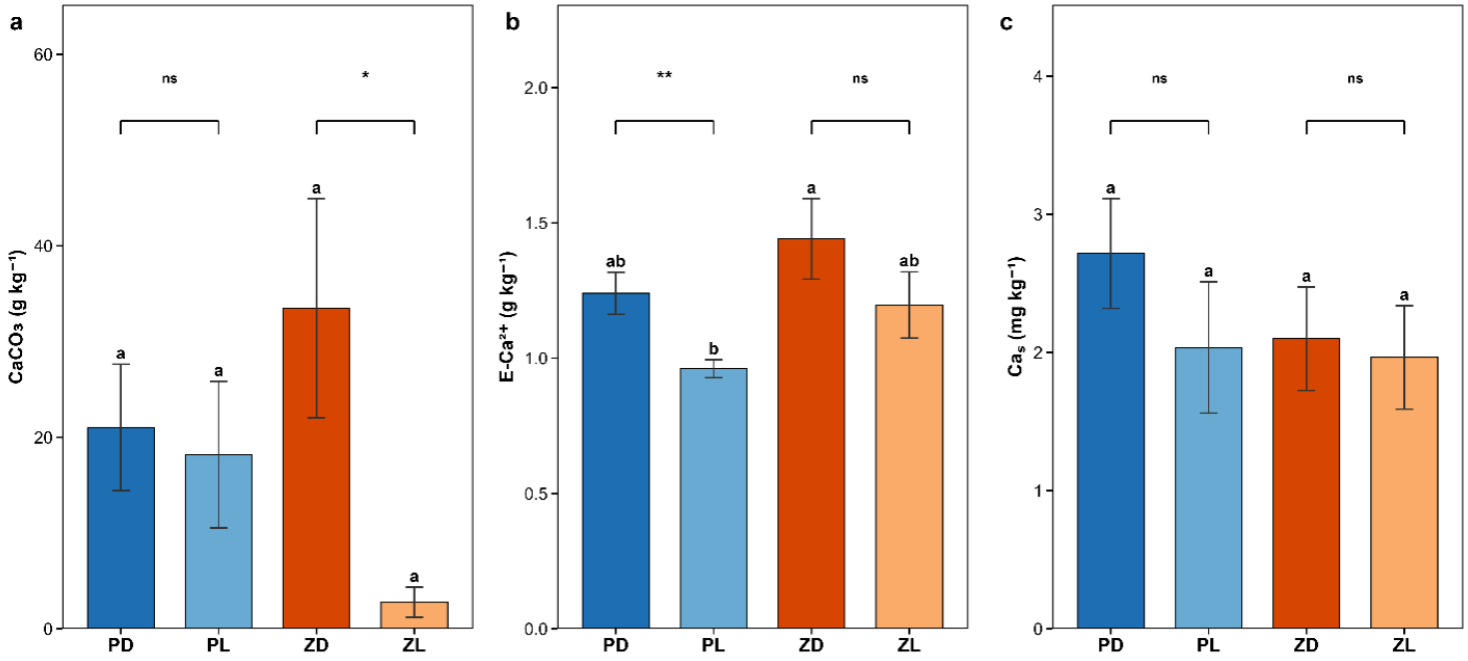


Figure 4

Calcium fractions across the four site–lithology treatments (n = 9 per treatment): (a) calcium carbonate ($CaCO_3$), (b) exchangeable Ca^{2+} (E-Ca^{2+}), and (c) sulfate-extractable Ca (Ca□). Bars represent mean ± SE. Different lowercase letters indicate significant differences among treatments ($p < 0.05$, LSD test). Asterisks denote significant differences between Dolomite and Limestone within the same site (independent-samples t-test; *p < 0.05; **p < 0.01; ***p < 0.001; ns, not significant).

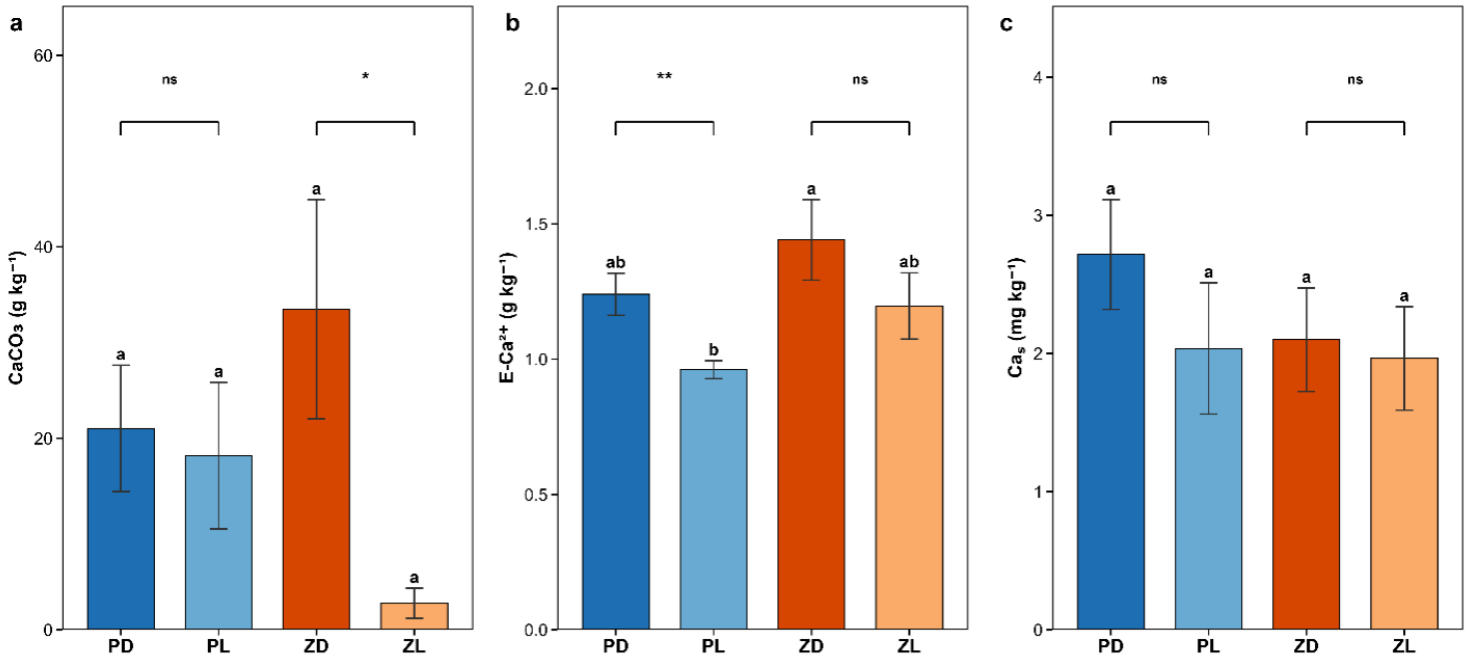


Figure 4

Calcium fractions across the four site–lithology treatments (n = 9 per treatment): (a) calcium carbonate ($CaCO_3$), (b) exchangeable Ca^{2+} (E-Ca^{2+}), and (c) sulfate-extractable Ca (Ca□). Bars represent mean ± SE. Different lowercase letters indicate significant differences among treatments ($p < 0.05$, LSD test). Asterisks denote significant differences between Dolomite and Limestone within the same site (independent-samples t-test; *$p < 0.05$; **$p < 0.01$; ***$p < 0.001$; ns, not significant).

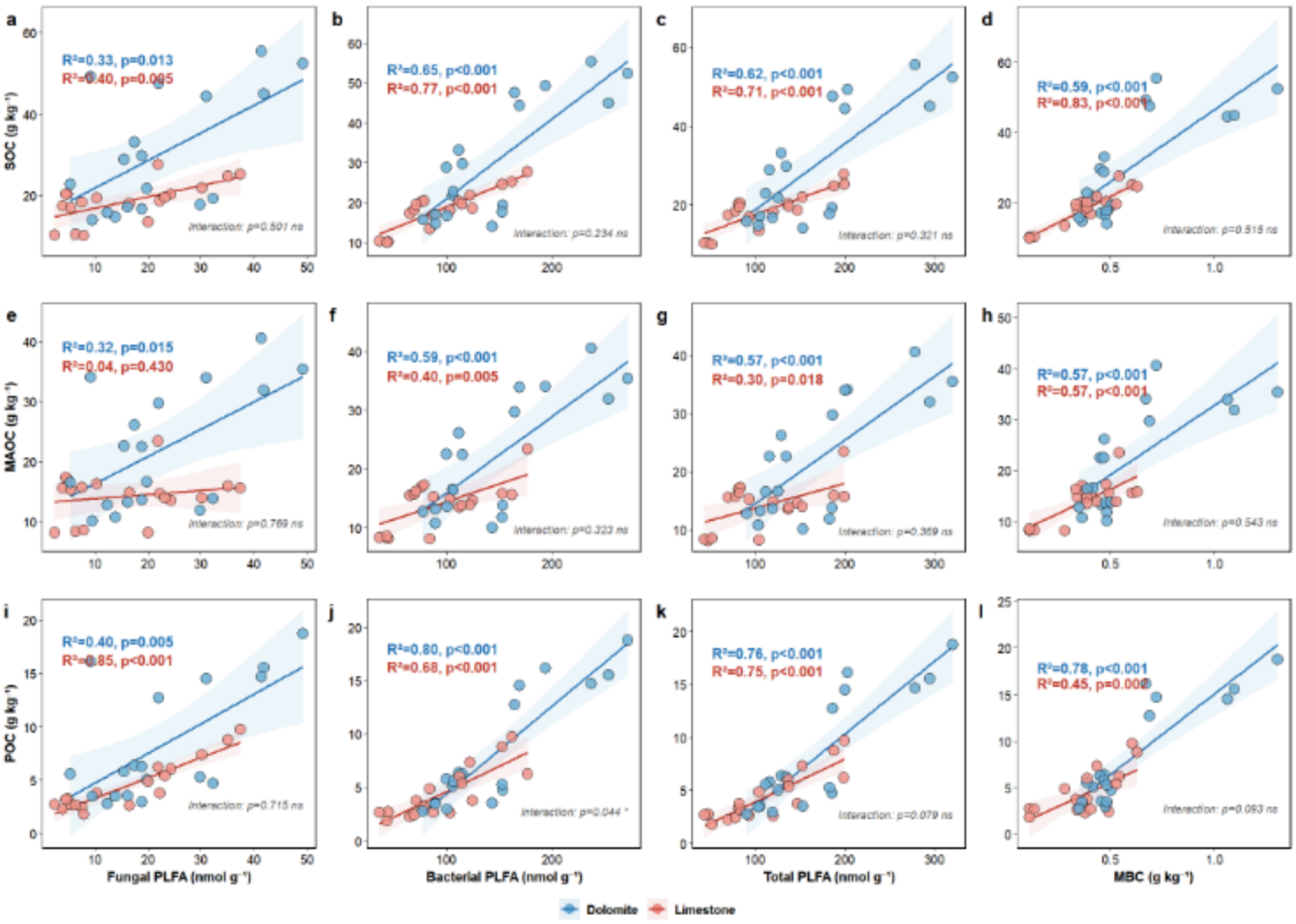


Figure 5

Relationships between microbial properties (fungal PLFA, bacterial PLFA, total PLFA, and MBC) and soil organic carbon (SOC), mineral-associated organic carbon (MAOC), and particulate organic carbon (POC) in Dolomite (blue) and Limestone (red) soils. Shaded bands represent 95% confidence intervals of the fitted linear regressions. R^2 and p-values are shown for each lithology; interaction p-values (bottom right of each panel) indicate whether the predictor–carbon relationship differed significantly between lithologies based on analysis of covariance (ANCOVA) controlling for site (*p < 0.05; **p < 0.01; ***p < 0.001; ns, not significant).

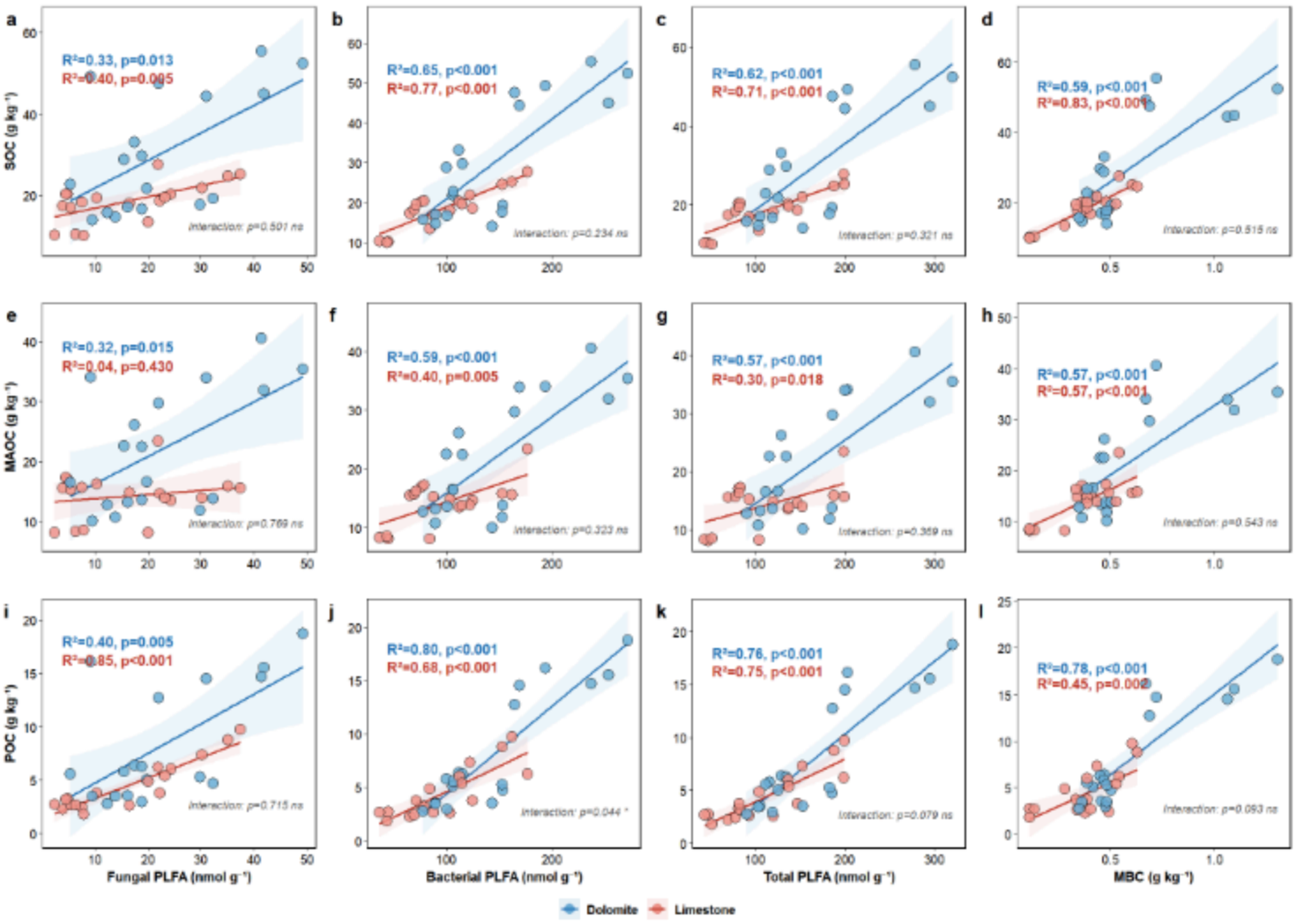


Figure 5

Relationships between microbial properties (fungal PLFA, bacterial PLFA, total PLFA, and MBC) and soil organic carbon (SOC), mineral-associated organic carbon (MAOC), and particulate organic carbon (POC) in Dolomite (blue) and Limestone (red) soils. Shaded bands represent 95% confidence intervals of the fitted linear regressions. R^2 and p-values are shown for each lithology; interaction p-values (bottom right of each panel) indicate whether the predictor–carbon relationship differed significantly between lithologies based on analysis of covariance (ANCOVA) controlling for site (*p < 0.05; **p < 0.01; ***p < 0.001; ns, not significant).

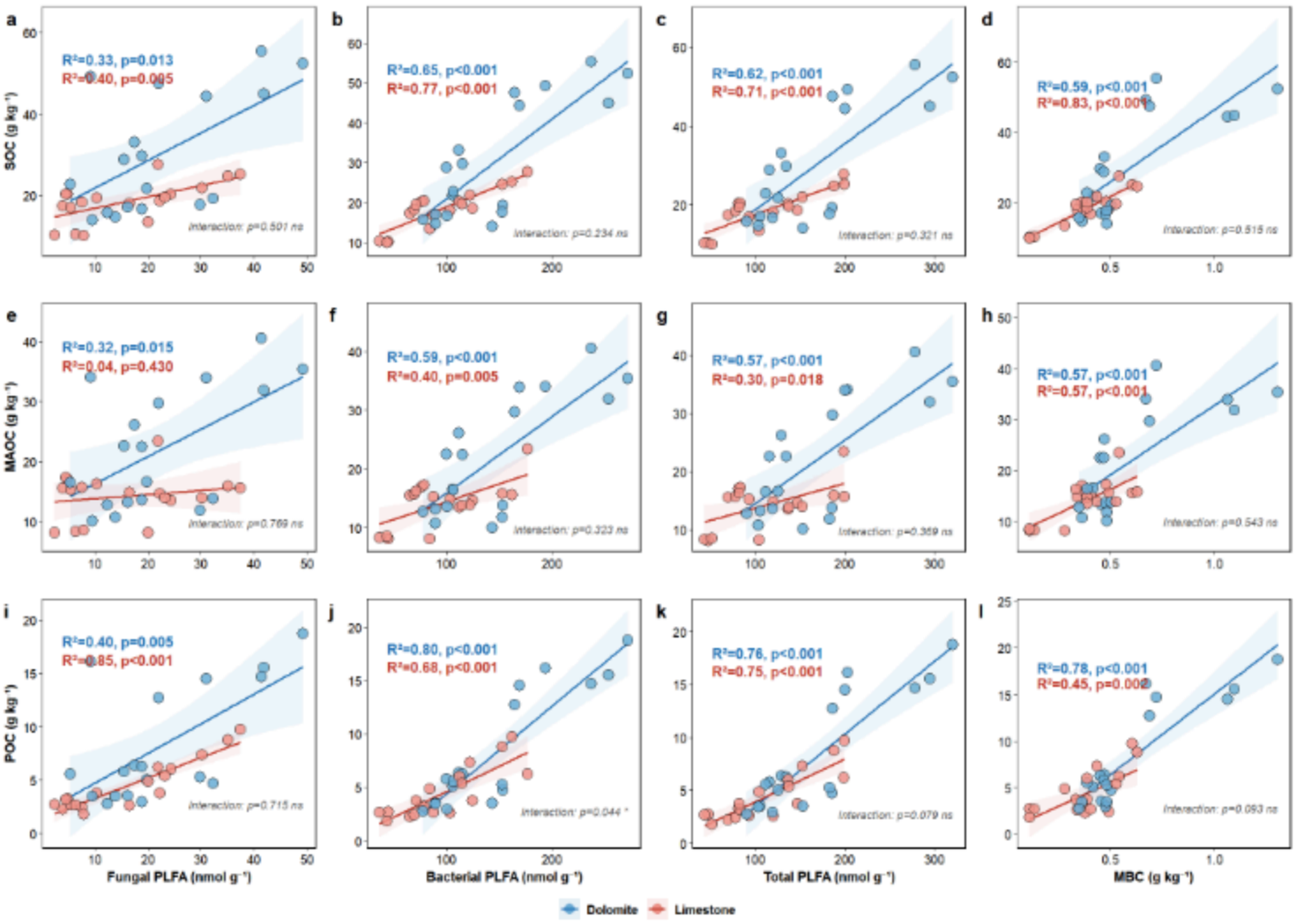


Figure 5

Relationships between microbial properties (fungal PLFA, bacterial PLFA, total PLFA, and MBC) and soil organic carbon (SOC), mineral-associated organic carbon (MAOC), and particulate organic carbon (POC) in Dolomite (blue) and Limestone (red) soils. Shaded bands represent 95% confidence intervals of the fitted linear regressions. R^2 and p-values are shown for each lithology; interaction p-values (bottom right of each panel) indicate whether the predictor–carbon relationship differed significantly between lithologies based on analysis of covariance (ANCOVA) controlling for site (*p < 0.05; **p < 0.01; ***p < 0.001; ns, not significant).

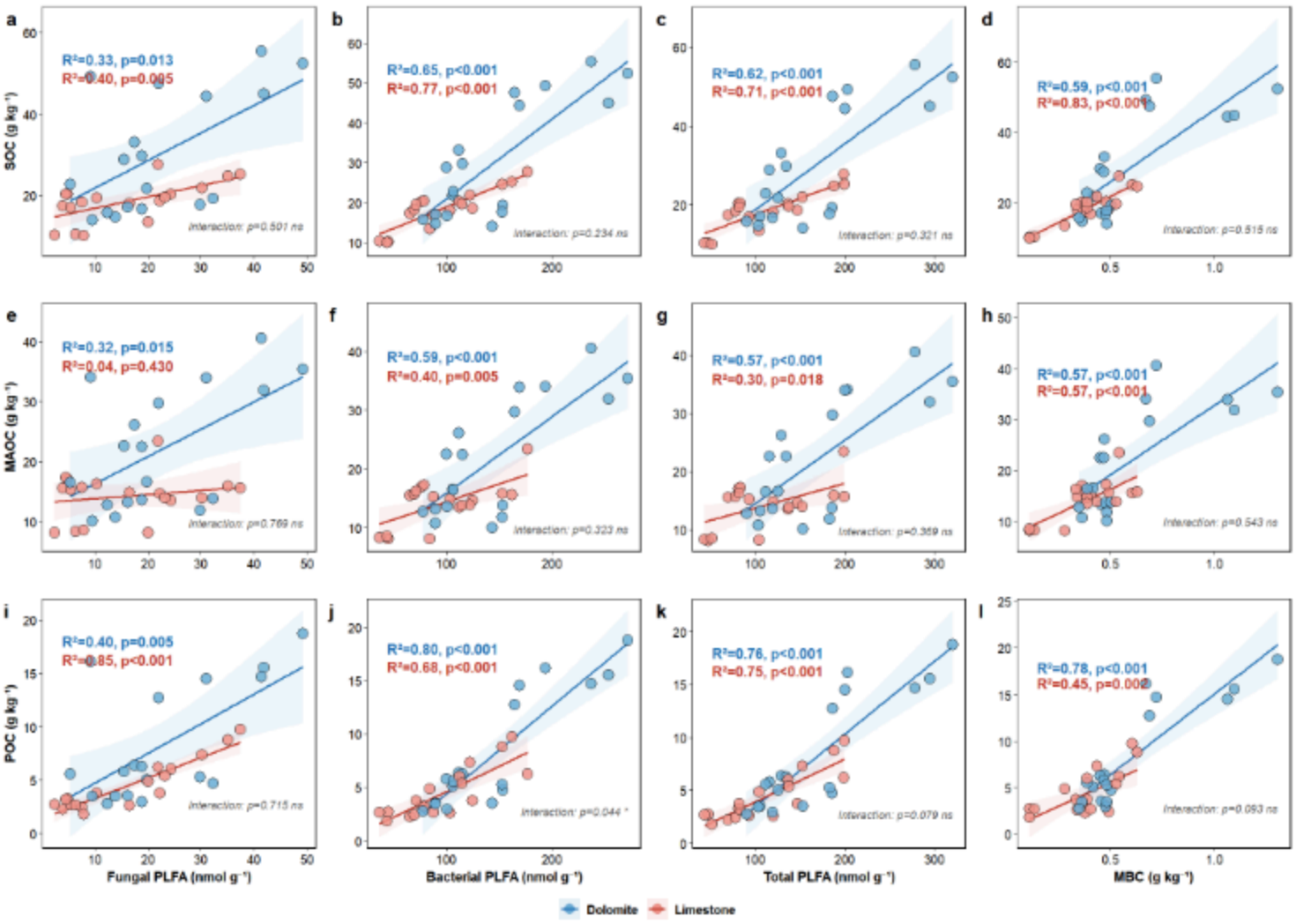


Figure 5

Relationships between microbial properties (fungal PLFA, bacterial PLFA, total PLFA, and MBC) and soil organic carbon (SOC), mineral-associated organic carbon (MAOC), and particulate organic carbon (POC) in Dolomite (blue) and Limestone (red) soils. Shaded bands represent 95% confidence intervals of the fitted linear regressions. R^2 and p-values are shown for each lithology; interaction p-values (bottom right of each panel) indicate whether the predictor–carbon relationship differed significantly between lithologies based on analysis of covariance (ANCOVA) controlling for site (*p < 0.05; **p < 0.01; ***p < 0.001; ns, not significant).

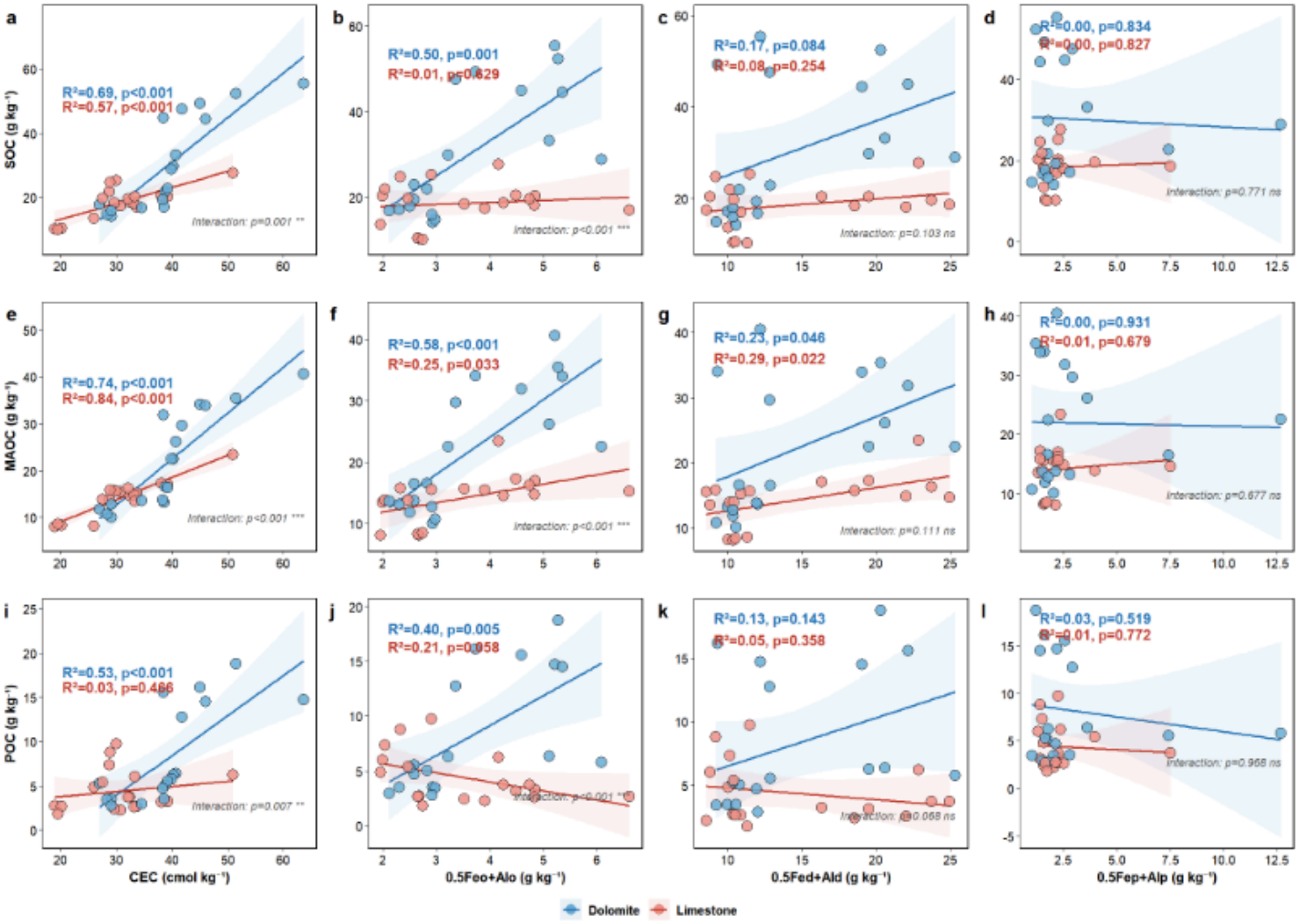


Figure 6

Relationships between mineral properties (CEC, 0.5Feo+Alo, 0.5Fed+Ald, and 0.5Fep+Alp) and soil organic carbon (SOC), mineral-associated organic carbon (MAOC), and particulate organic carbon (POC) in Dolomite (blue) and Limestone (red) soils. Shaded bands represent 95% confidence intervals of the fitted linear regressions. R^2 and p-values are shown for each lithology; interaction p-values (bottom right of each panel) indicate whether the predictor–carbon relationship differed significantly between lithologies based on analysis of covariance (ANCOVA) controlling for site (*p < 0.05; **p < 0.01; ***p < 0.001; ns, not significant).

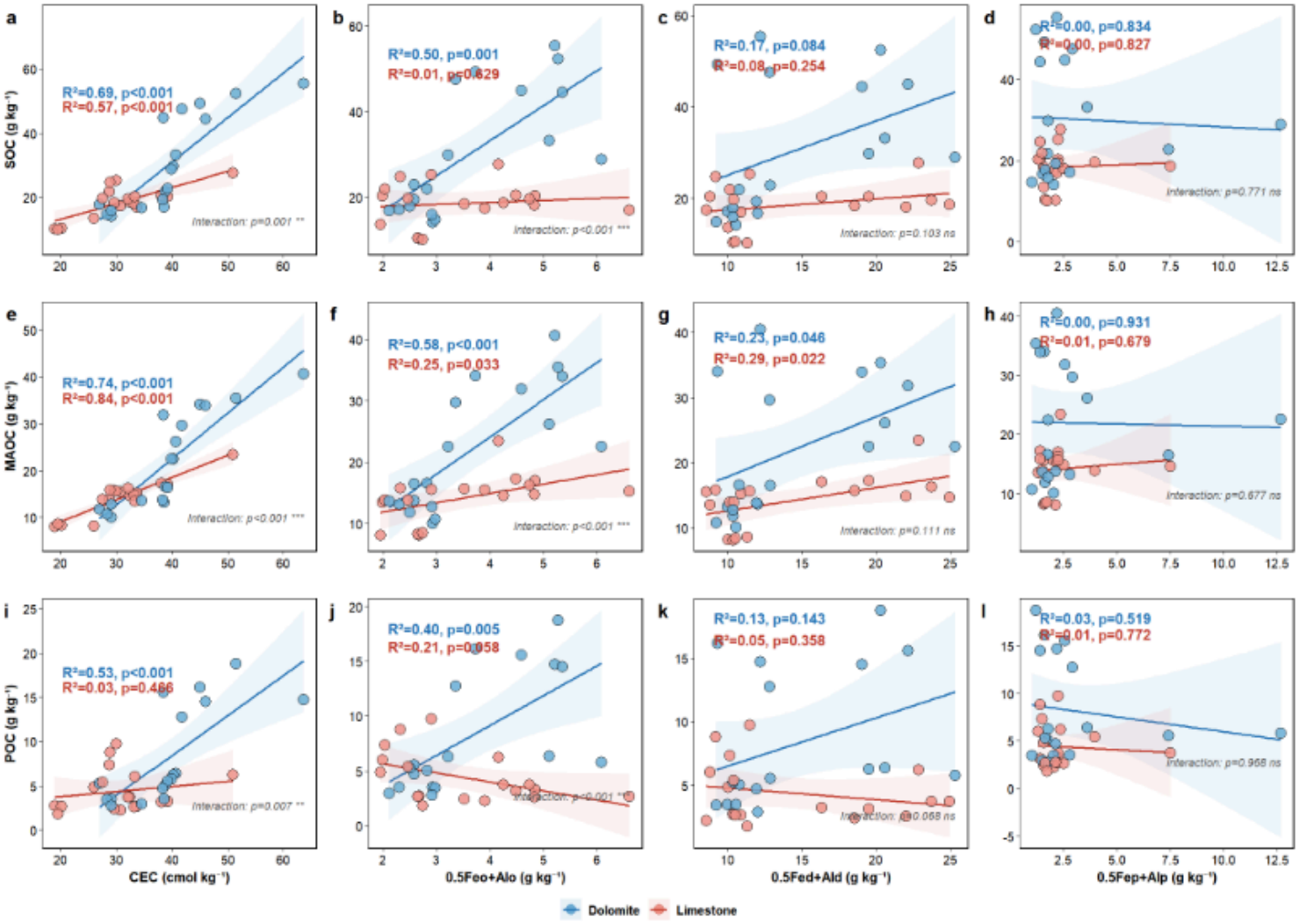


Figure 6

Relationships between mineral properties (CEC, 0.5Feo+Alo, 0.5Fed+Ald, and 0.5Fep+Alp) and soil organic carbon (SOC), mineral-associated organic carbon (MAOC), and particulate organic carbon (POC) in Dolomite (blue) and Limestone (red) soils. Shaded bands represent 95% confidence intervals of the fitted linear regressions. R^2 and p-values are shown for each lithology; interaction p-values (bottom right of each panel) indicate whether the predictor–carbon relationship differed significantly between lithologies based on analysis of covariance (ANCOVA) controlling for site (*p < 0.05; **p < 0.01; ***p < 0.001; ns, not significant).

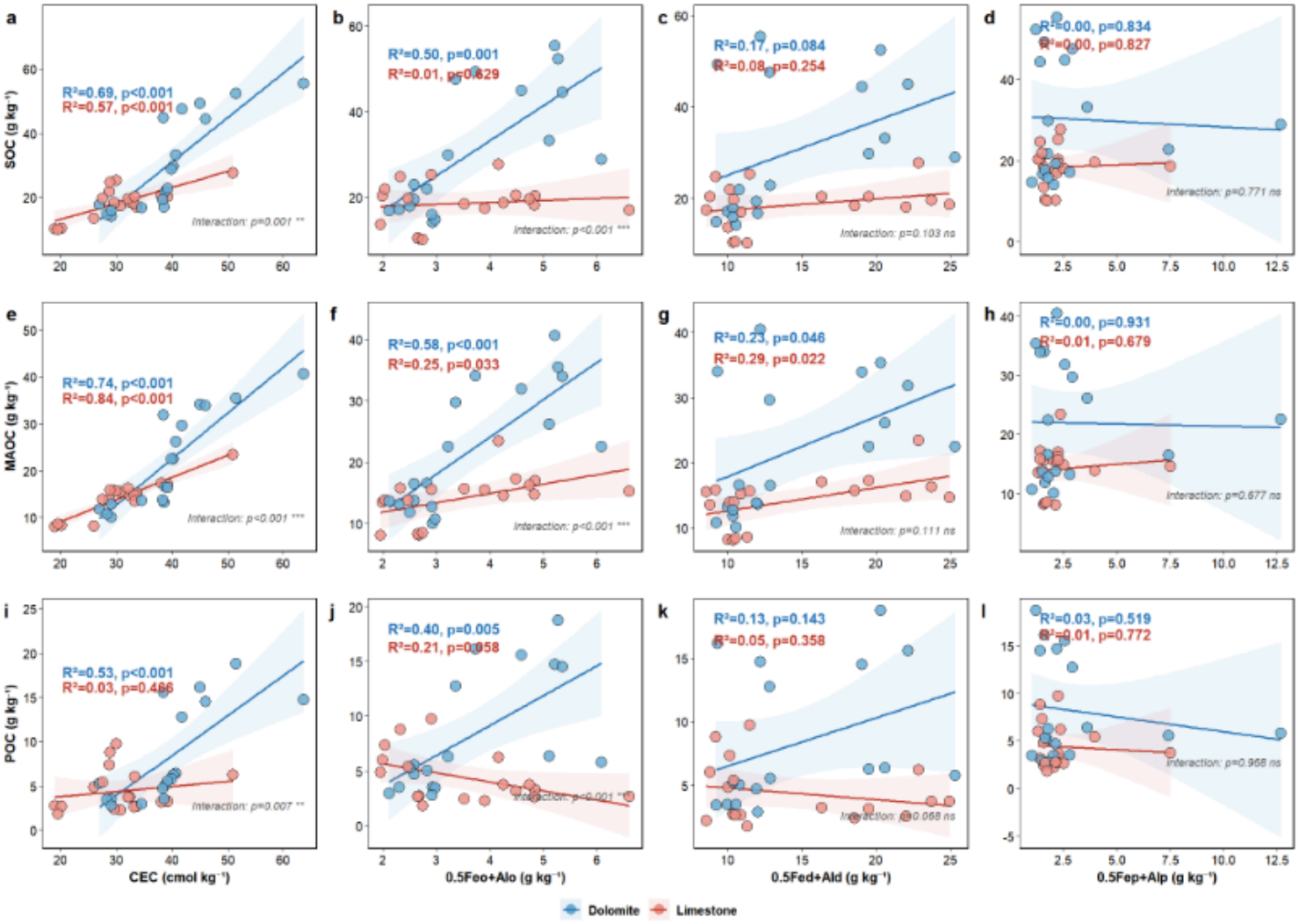


Figure 6

Relationships between mineral properties (CEC, 0.5Feo+Alo, 0.5Fed+Ald, and 0.5Fep+Alp) and soil organic carbon (SOC), mineral-associated organic carbon (MAOC), and particulate organic carbon (POC) in Dolomite (blue) and Limestone (red) soils. Shaded bands represent 95% confidence intervals of the fitted linear regressions. R^2 and p-values are shown for each lithology; interaction p-values (bottom right of each panel) indicate whether the predictor–carbon relationship differed significantly between lithologies based on analysis of covariance (ANCOVA) controlling for site (*p < 0.05; **p < 0.01; ***p < 0.001; ns, not significant).

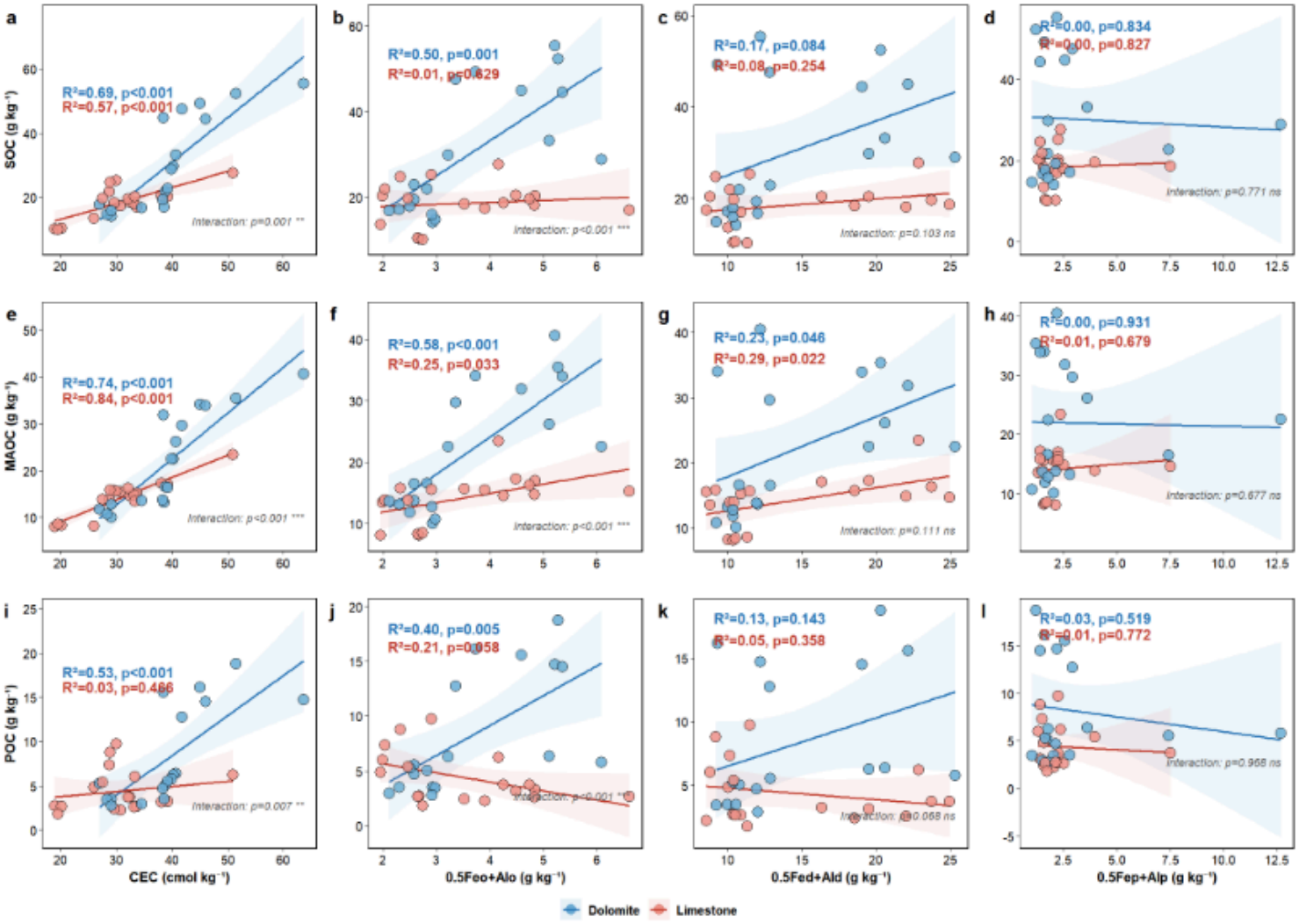


Figure 6

Relationships between mineral properties (CEC, 0.5Feo+Alo, 0.5Fed+Ald, and 0.5Fep+Alp) and soil organic carbon (SOC), mineral-associated organic carbon (MAOC), and particulate organic carbon (POC) in Dolomite (blue) and Limestone (red) soils. Shaded bands represent 95% confidence intervals of the fitted linear regressions. R^2 and p-values are shown for each lithology; interaction p-values (bottom right of each panel) indicate whether the predictor–carbon relationship differed significantly between lithologies based on analysis of covariance (ANCOVA) controlling for site (*p < 0.05; **p < 0.01; ***p < 0.001; ns, not significant).

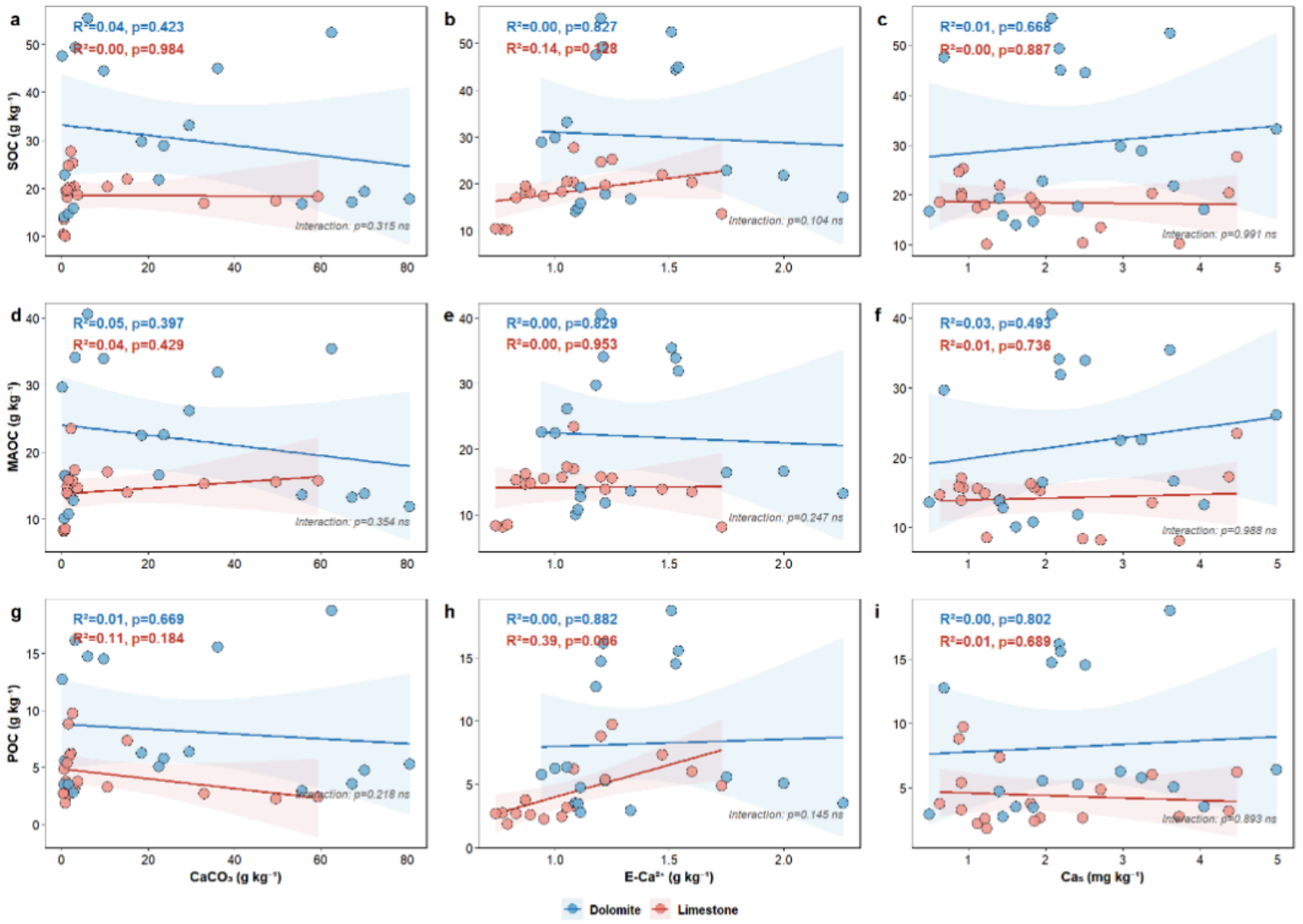


Figure 7

Relationships between calcium fractions ($CaCO_3$, exchangeable Ca^{2+}, and sulfate-extractable Ca) and soil organic carbon (SOC), mineral-associated organic carbon (MAOC), and particulate organic carbon (POC) in Dolomite (blue) and Limestone (red) soils. Shaded bands represent 95% confidence intervals of the fitted linear regressions. R^2 and p-values are shown for each lithology; interaction p-values (bottom right of each panel) indicate whether the predictor–carbon relationship differed significantly between lithologies based on analysis of covariance (ANCOVA) controlling for site (*p < 0.05; **p < 0.01; ***p < 0.001; ns, not significant).

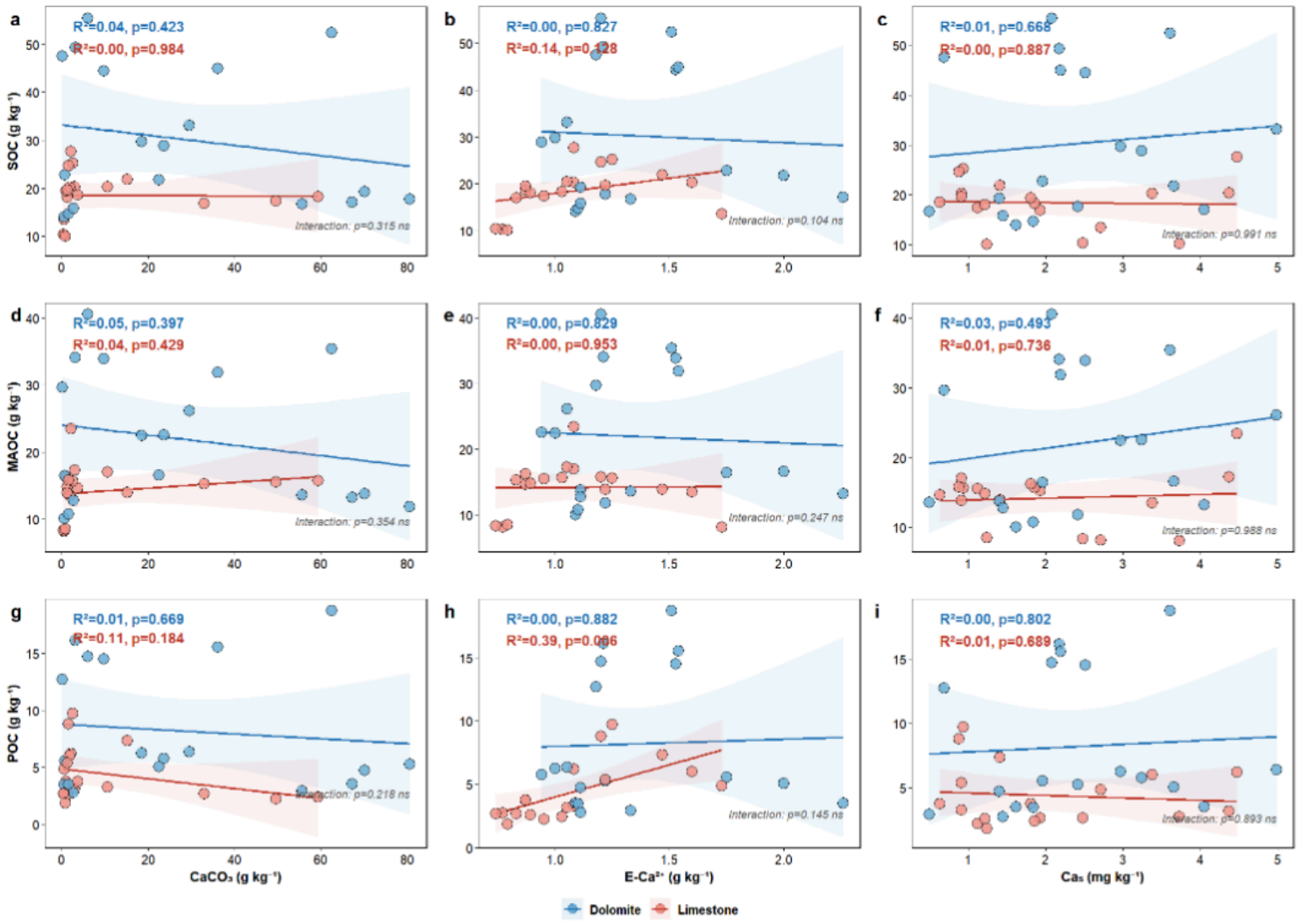


Figure 7

Relationships between calcium fractions ($CaCO_3$, exchangeable Ca^{2+}, and sulfate-extractable Ca) and soil organic carbon (SOC), mineral-associated organic carbon (MAOC), and particulate organic carbon (POC) in Dolomite (blue) and Limestone (red) soils. Shaded bands represent 95% confidence intervals of the fitted linear regressions. R^2 and p-values are shown for each lithology; interaction p-values (bottom right of each panel) indicate whether the predictor–carbon relationship differed significantly between lithologies based on analysis of covariance (ANCOVA) controlling for site (*p < 0.05; **p < 0.01; ***p < 0.001; ns, not significant).

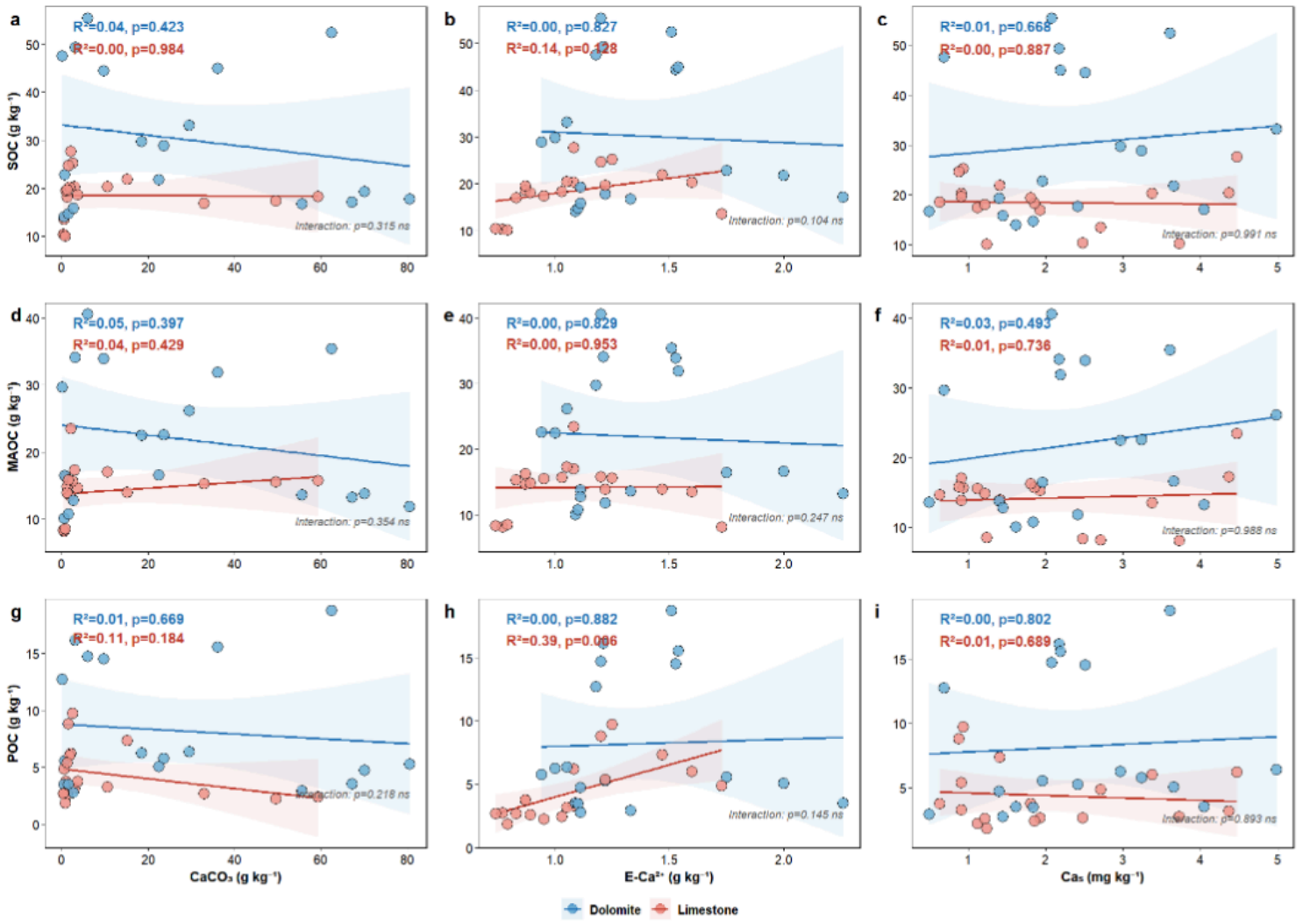


Figure 7

Relationships between calcium fractions ($CaCO_3$, exchangeable Ca^{2+}, and sulfate-extractable Ca) and soil organic carbon (SOC), mineral-associated organic carbon (MAOC), and particulate organic carbon (POC) in Dolomite (blue) and Limestone (red) soils. Shaded bands represent 95% confidence intervals of the fitted linear regressions. R^2 and p-values are shown for each lithology; interaction p-values (bottom right of each panel) indicate whether the predictor–carbon relationship differed significantly between lithologies based on analysis of covariance (ANCOVA) controlling for site (*p < 0.05; **p < 0.01; ***p < 0.001; ns, not significant).

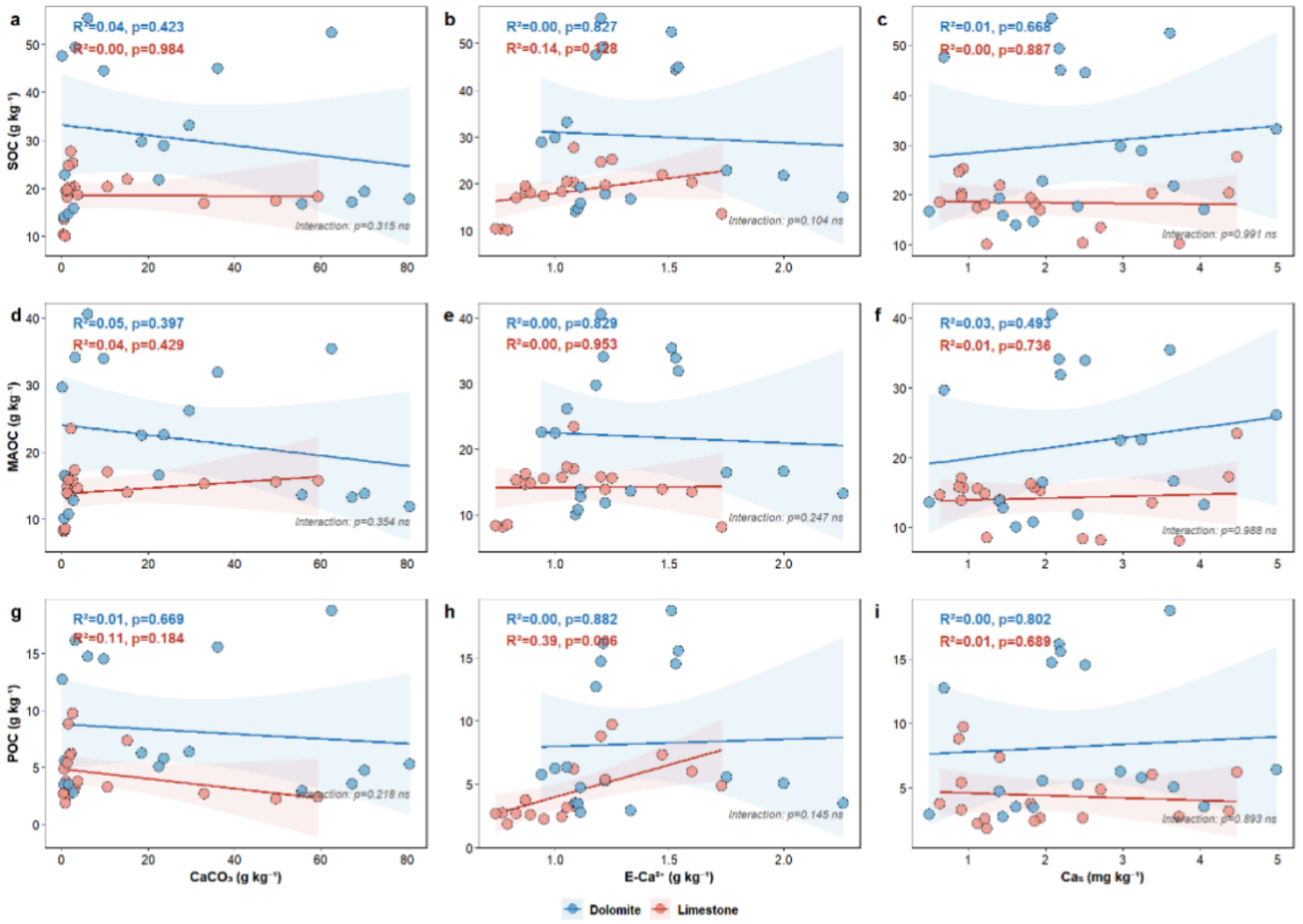


Figure 7

Relationships between calcium fractions ($CaCO_3$, exchangeable Ca^{2+}, and sulfate-extractable Ca) and soil organic carbon (SOC), mineral-associated organic carbon (MAOC), and particulate organic carbon (POC) in Dolomite (blue) and Limestone (red) soils. Shaded bands represent 95% confidence intervals of the fitted linear regressions. R^2 and p-values are shown for each lithology; interaction p-values (bottom right of each panel) indicate whether the predictor–carbon relationship differed significantly between lithologies based on analysis of covariance (ANCOVA) controlling for site (*p < 0.05; **p < 0.01; ***p < 0.001; ns, not significant).

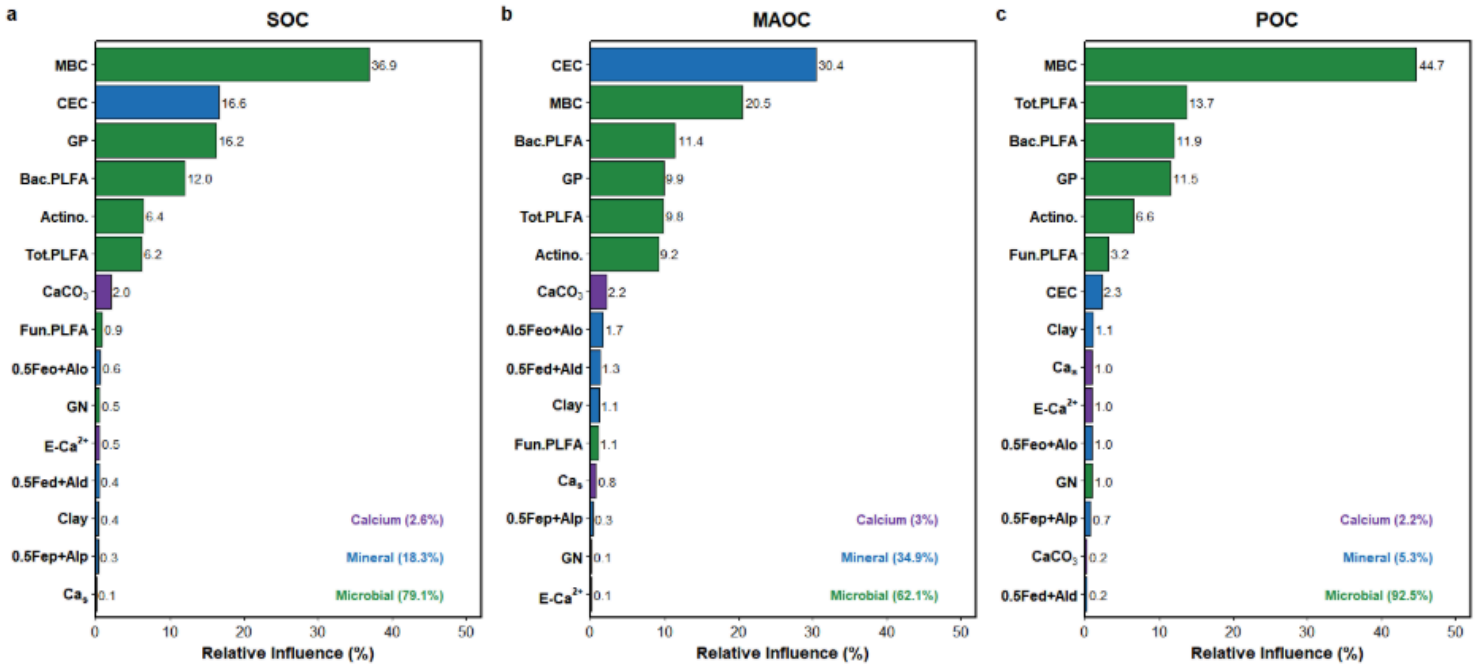


Figure 8

Relative importance of calcium, mineral, and microbial predictor groups for (a) soil organic carbon (SOC), (b) mineral-associated organic carbon (MAOC), and (c) particulate organic carbon (POC), determined by boosted regression tree (BRT) analysis. Horizontal bars show the relative influence (%) of individual predictors, ranked from highest to lowest. Group totals (Calcium, Mineral, Microbial) are indicated in the bottom-right corner of each panel. $CaCO_3$, calcium carbonate; Ca□, sulfate-extractable Ca; E-Ca^{2+}, exchangeable Ca^{2+}; CEC, cation exchange capacity; (0.5Feo+Alo), oxalate-extractable Fe–Al; (0.5Fed+Ald), dithionite-extractable Fe–Al; (0.5Fep+Alp), pyrophosphate-extractable Fe–Al; MBC, microbial biomass carbon; FunPLFA, fungal phospholipid fatty acid; BacPLFA, bacterial phospholipid fatty acid; TotalPLFA, total phospholipid fatty acid; GP, Gram-positive bacteria; GN, Gram-negative bacteria; Actinomycetes.

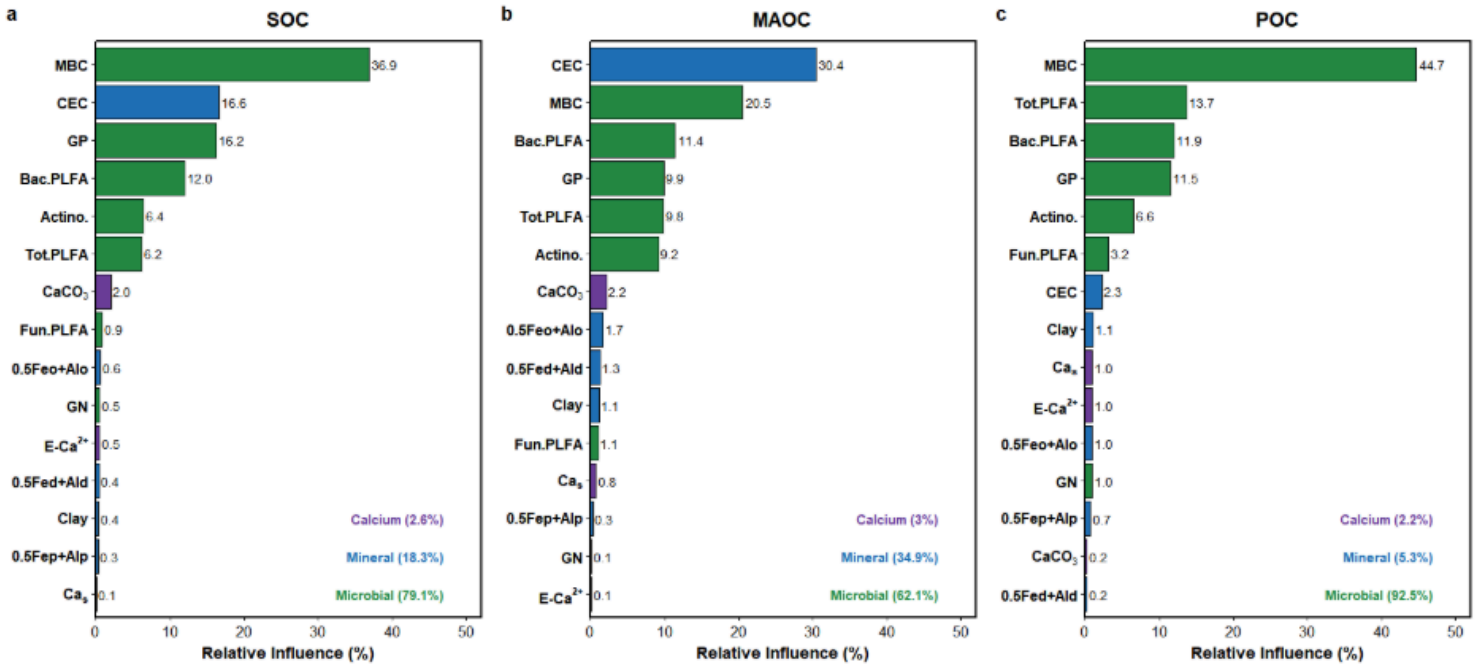


Figure 8

Relative importance of calcium, mineral, and microbial predictor groups for (a) soil organic carbon (SOC), (b) mineral-associated organic carbon (MAOC), and (c) particulate organic carbon (POC), determined by boosted regression tree (BRT) analysis. Horizontal bars show the relative influence (%) of individual predictors, ranked from highest to lowest. Group totals (Calcium, Mineral, Microbial) are indicated in the bottom-right corner of each panel. $CaCO_3$, calcium carbonate; Ca□, sulfate-extractable Ca; E-Ca^{2+}, exchangeable Ca^{2+}; CEC, cation exchange capacity; (0.5Feo+Alo), oxalate-extractable Fe–Al; (0.5Fed+Ald), dithionite-extractable Fe–Al; (0.5Fep+Alp), pyrophosphate-extractable Fe–Al; MBC, microbial biomass carbon; FunPLFA, fungal phospholipid fatty acid; BacPLFA, bacterial phospholipid fatty acid; TotalPLFA, total phospholipid fatty acid; GP, Gram-positive bacteria; GN, Gram-negative bacteria; Actinomycetes.

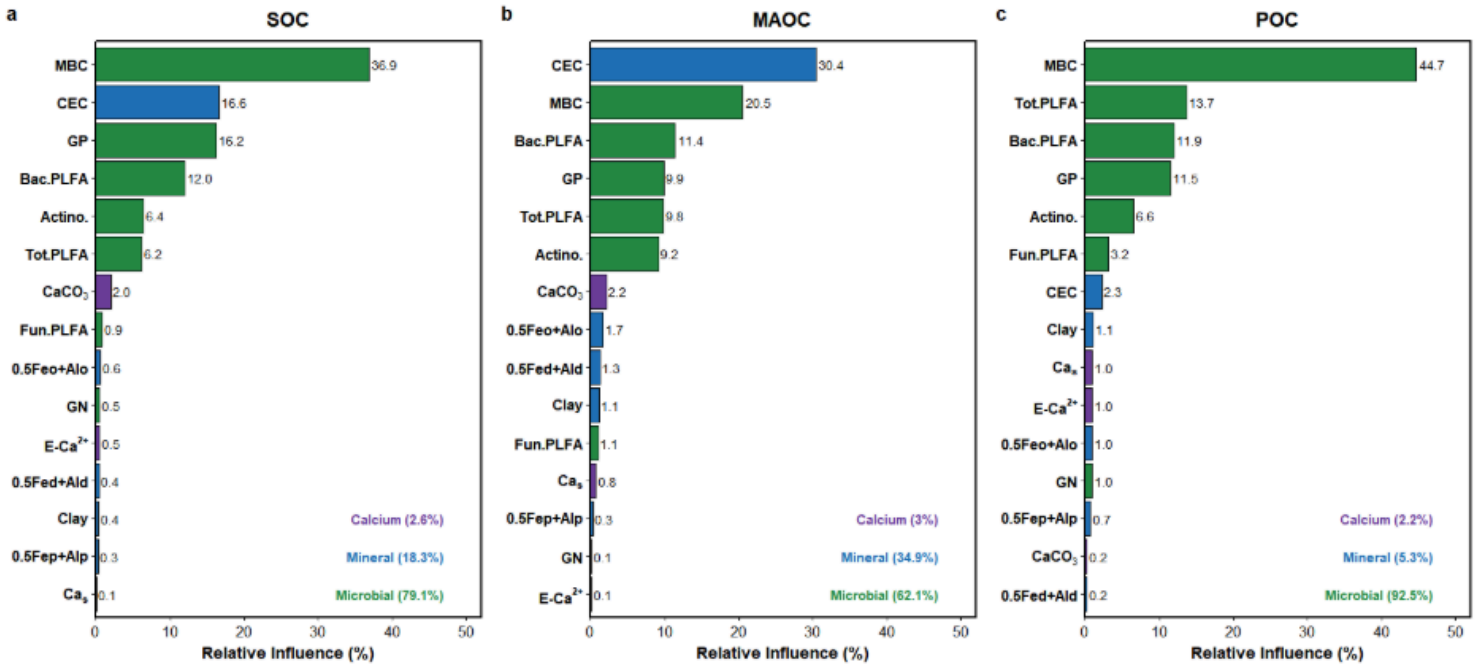


Figure 8

Relative importance of calcium, mineral, and microbial predictor groups for (a) soil organic carbon (SOC), (b) mineral-associated organic carbon (MAOC), and (c) particulate organic carbon (POC), determined by boosted regression tree (BRT) analysis. Horizontal bars show the relative influence (%) of individual predictors, ranked from highest to lowest. Group totals (Calcium, Mineral, Microbial) are indicated in the bottom-right corner of each panel. $CaCO_3$, calcium carbonate; Ca□, sulfate-extractable Ca; E-Ca^{2+}, exchangeable Ca^{2+}; CEC, cation exchange capacity; (0.5Feo+Alo), oxalate-extractable Fe–Al; (0.5Fed+Ald), dithionite-extractable Fe–Al; (0.5Fep+Alp), pyrophosphate-extractable Fe–Al; MBC, microbial biomass carbon; FunPLFA, fungal phospholipid fatty acid; BacPLFA, bacterial phospholipid fatty acid; TotalPLFA, total phospholipid fatty acid; GP, Gram-positive bacteria; GN, Gram-negative bacteria; Actinomycetes.

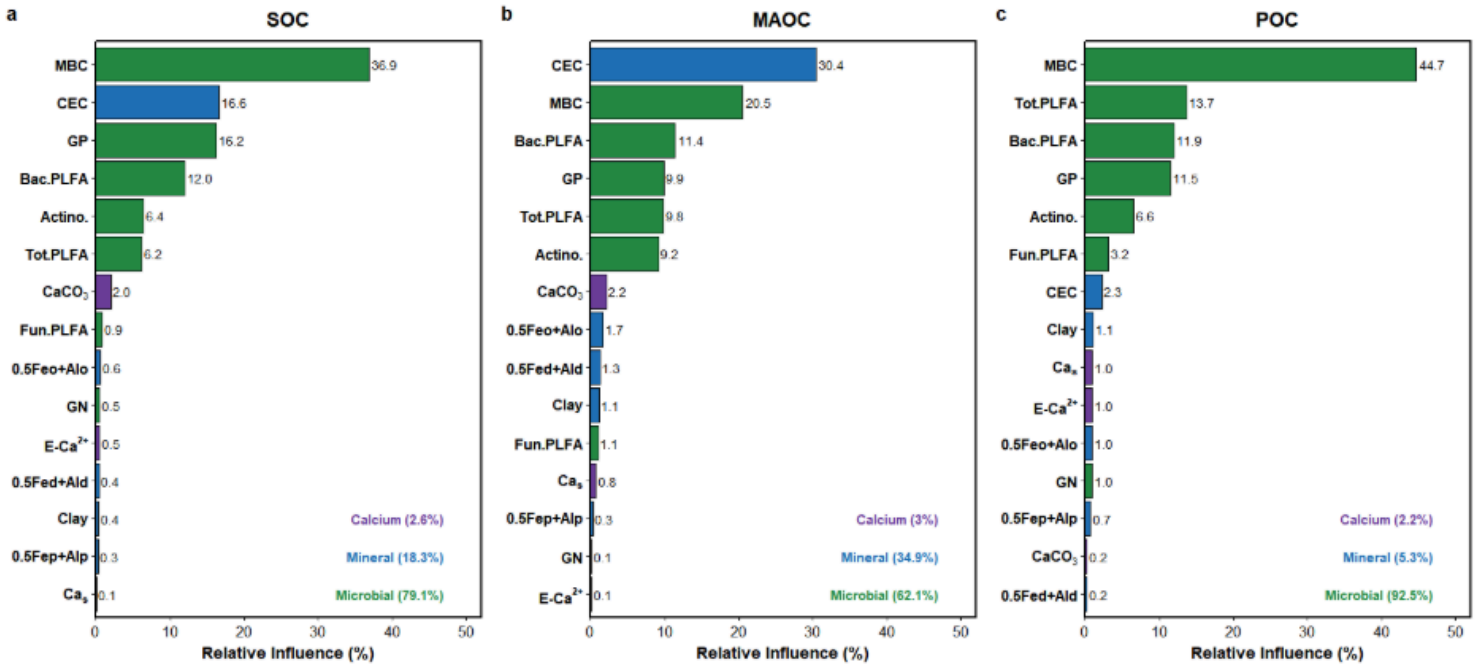


Figure 8

Relative importance of calcium, mineral, and microbial predictor groups for (a) soil organic carbon (SOC), (b) mineral-associated organic carbon (MAOC), and (c) particulate organic carbon (POC), determined by boosted regression tree (BRT) analysis. Horizontal bars show the relative influence (%) of individual predictors, ranked from highest to lowest. Group totals (Calcium, Mineral, Microbial) are indicated in the bottom-right corner of each panel. $CaCO_3$, calcium carbonate; Ca□, sulfate-extractable Ca; E-Ca^{2+}, exchangeable Ca^{2+}; CEC, cation exchange capacity; (0.5Feo+Alo), oxalate-extractable Fe–Al; (0.5Fed+Ald), dithionite-extractable Fe–Al; (0.5Fep+Alp), pyrophosphate-extractable Fe–Al; MBC, microbial biomass carbon; FunPLFA, fungal phospholipid fatty acid; BacPLFA, bacterial phospholipid fatty acid; TotalPLFA, total phospholipid fatty acid; GP, Gram-positive bacteria; GN, Gram-negative bacteria; Actinomycetes.

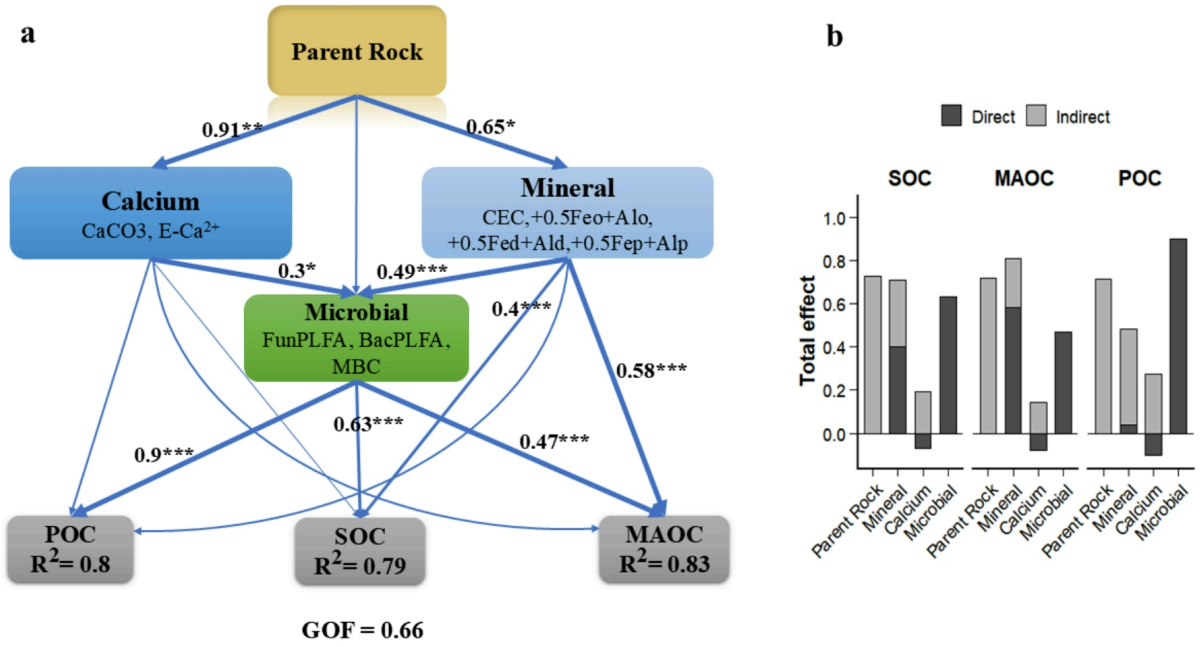


Figure 9

(a) Partial least squares structural equation model (PLS-SEM) showing direct and indirect pathways among parent rock type, calcium properties, mineral properties, microbial properties, and soil carbon fractions (SOC, MAOC, POC). Solid arrows indicate significant standardized path coefficients ($p < 0.05$); thin arrows indicate non-significant paths. Path coefficients (β) are shown alongside each arrow. Goodness-of-fit (GOF) and variance explained (R^2) for each carbon fraction are reported within the figure. (b) Total effects (direct + indirect) on SOC, MAOC and POC. SOC, soil organic carbon; POC, particulate organic carbon; MAOC, mineral-associated organic carbon; CEC, cation exchange capacity; $CaCO_3$, calcium carbonate; E-Ca^{2+}, exchangeable Ca^{2+}; MBC, microbial biomass carbon; BacPLFA, bacterial phospholipid fatty acid; FunPLFA, fungal phospholipid fatty acid; (0.5Feo+Alo), oxalate-extractable Fe–Al; (0.5Fed+Ald), dithionite-extractable Fe–Al.

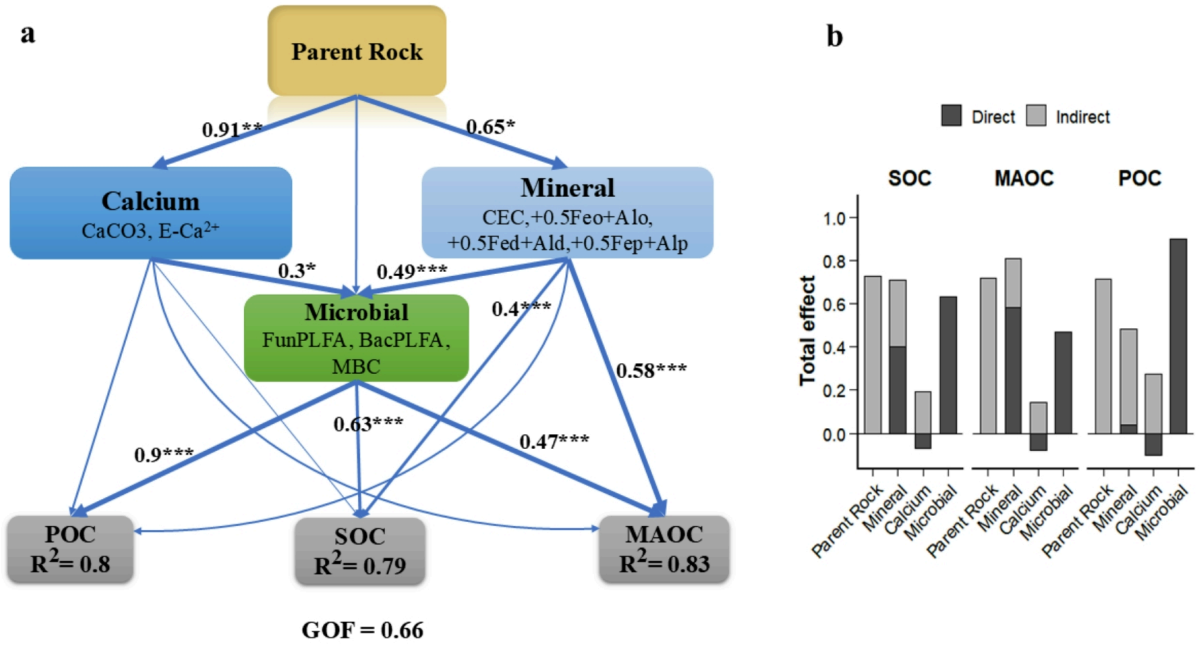


Figure 9

(a) Partial least squares structural equation model (PLS-SEM) showing direct and indirect pathways among parent rock type, calcium properties, mineral properties, microbial properties, and soil carbon fractions (SOC, MAOC, POC). Solid arrows indicate significant standardized path coefficients ($p < 0.05$); thin arrows indicate non-significant paths. Path coefficients (β) are shown alongside each arrow. Goodness-of-fit (GOF) and variance explained (R^2) for each carbon fraction are reported within the figure. (b) Total effects (direct + indirect) on SOC, MAOC and POC. SOC, soil organic carbon; POC, particulate organic carbon; MAOC, mineral-associated organic carbon; CEC, cation exchange capacity; $CaCO_3$, calcium carbonate; E-Ca^{2+}, exchangeable Ca^{2+}; MBC, microbial biomass carbon; BacPLFA, bacterial phospholipid fatty acid; FunPLFA, fungal phospholipid fatty acid; (0.5Feo+Alo), oxalate-extractable Fe–Al; (0.5Fed+Ald), dithionite-extractable Fe–Al.

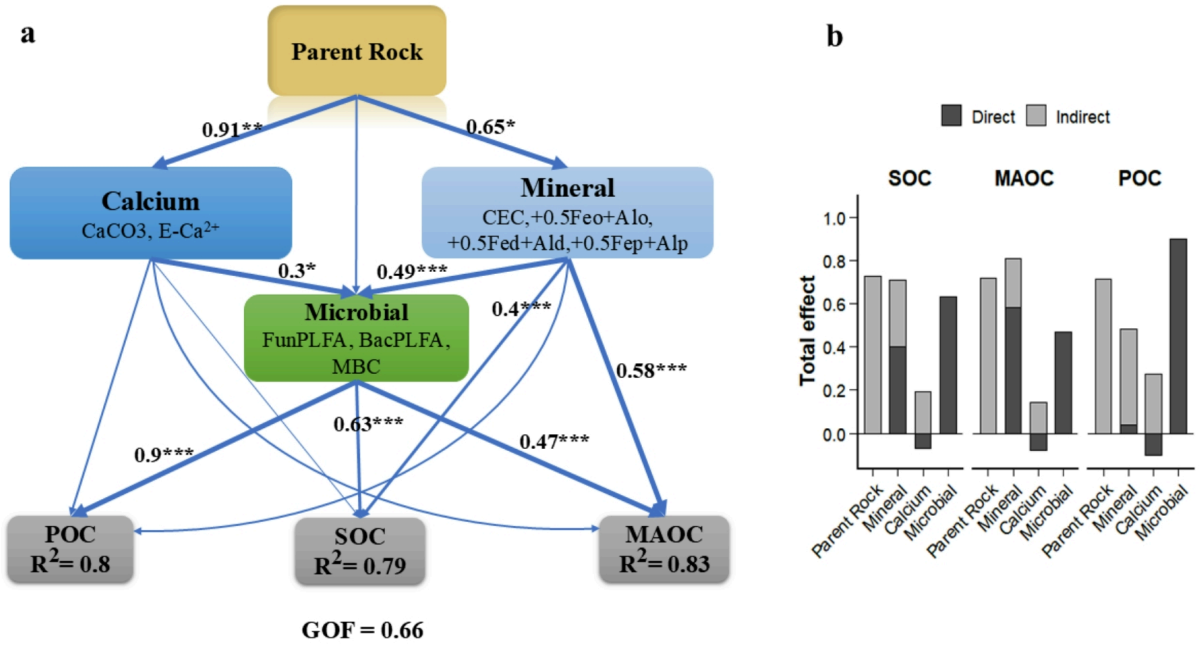


Figure 9

(a) Partial least squares structural equation model (PLS-SEM) showing direct and indirect pathways among parent rock type, calcium properties, mineral properties, microbial properties, and soil carbon fractions (SOC, MAOC, POC). Solid arrows indicate significant standardized path coefficients ($p < 0.05$); thin arrows indicate non-significant paths. Path coefficients (β) are shown alongside each arrow. Goodness-of-fit (GOF) and variance explained (R^2) for each carbon fraction are reported within the figure. (b) Total effects (direct + indirect) on SOC, MAOC and POC. SOC, soil organic carbon; POC, particulate organic carbon; MAOC, mineral-associated organic carbon; CEC, cation exchange capacity; $CaCO_3$, calcium carbonate; E-Ca^{2+}, exchangeable Ca^{2+}; MBC, microbial biomass carbon; BacPLFA, bacterial phospholipid fatty acid; FunPLFA, fungal phospholipid fatty acid; (0.5Feo+Alo), oxalate-extractable Fe–Al; (0.5Fed+Ald), dithionite-extractable Fe–Al.

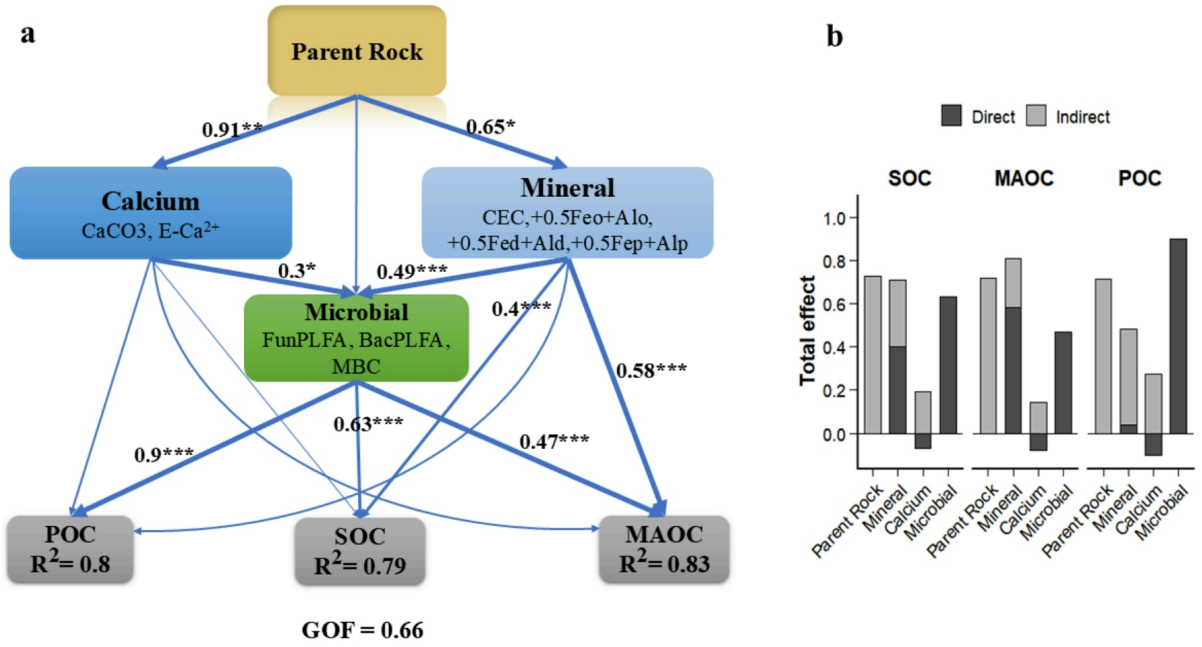


Figure 9

(a) Partial least squares structural equation model (PLS-SEM) showing direct and indirect pathways among parent rock type, calcium properties, mineral properties, microbial properties, and soil carbon fractions (SOC, MAOC, POC). Solid arrows indicate significant standardized path coefficients ($p < 0.05$); thin arrows indicate non-significant paths. Path coefficients (β) are shown alongside each arrow. Goodness-of-fit (GOF) and variance explained (R^2) for each carbon fraction are reported within the figure. (b) Total effects (direct + indirect) on SOC, MAOC and POC. SOC, soil organic carbon; POC, particulate organic carbon; MAOC, mineral-associated organic carbon; CEC, cation exchange capacity; $CaCO_3$, calcium carbonate; E-Ca^{2+}, exchangeable Ca^{2+}; MBC, microbial biomass carbon; BacPLFA, bacterial phospholipid fatty acid; FunPLFA, fungal phospholipid fatty acid; (0.5Feo+Alo), oxalate-extractable Fe–Al; (0.5Fed+Ald), dithionite-extractable Fe–Al.

Supplementary Files

This is a list of supplementary files associated with this preprint. Click to download.

- ESM1.pdf

- ESM1.pdf
- ESM1.pdf
- ESM1.pdf